Alma Mater Studiorum - Università Di Bologna

SECONDA FACOLTA' DI INGEGNERIA

Dottorato Di Ricerca In
Meccanica E Scienze Avanzate Dell'Ingegneria

Progetto N. 1: Disegno E Metodi Dell'Ingegneria Industriale E Scienze Aerospaziali

Ciclo XXIV

Settore scientifico disciplinare di afferenza: ING-IND/05

Coordinatore: Vincenzo Parenti Castelli

Design And Implementation Of An End-To-End Simulator For The BepiColombo Rotation Experiment

CANDIDATO

Alessandra Palli

RELATORE

Prof. Paolo Tortora

Anno 2012

“Mai ti è dato un desiderio senza che ti sia dato anche il potere di realizzarlo.”

Un ponte sull’eternità ***(Richard Bach)***

«Certo che ti farò del male. Certo che me ne farai.
Certo che ce ne faremo.
Ma questa è la condizione stessa dell’esistenza.
Farsi primavera, significa accettare il rischio dell’inverno.
Farsi presenza, significa accettare il rischio dell’assenza».

Antoine de Saint-Exupéry

Table of Contents

List of Figures

List of Tables

Acronyms

AWVR	Advanced Water Vapour Radiometer
BELA	BepiColombo Laser Altimeter
CVG	Computer Vision Group
DEIS	Dipartimento di Elettronica, Informatica e Sistemistica
DEM	Digital Elevation Module
DSA	Deep Space Antenna
DSN	Deep Space Network
DSS	Deep Space Station
ESA	European Space Agency
ESTRACK	ESA Tracking Station Network
GNSS	Global Navigation Satellite System
HRIC	High Resolution Imaging Channel
IR	Infrared
ISA	Italian Spring Accelerometer
KaT	Ka-band Transponder
MESSENGER	MErcury Surface, Space ENvironment, GEochemistry, and Ranging mission
MORE	Mercury Orbiter Radio science Experiment
MPO	Mercury Planetary Orbiter
NASA	National Aeronautics and Space Administration
S/C	Spacecraft
SEP	Sun-Earth-Probe
SIMBIO-SYS	Spectrometer and Imagers for MPO Bepicolombo Integrated Observatory – SYStem
SNR	Signal-to-Noise Ratio
S/W	Software
WBRS	Wide Band Ranging System
WVR	Water Vapour Radiometer

Chapter 1

Introduction

Introduction

The present work describes the PhD research activity that was carried out in the frame of the Radio Science Experiment, one of the payloads hosted on board the BepiColombo mission of the European Space Agency developed for the exploration of planet Mercury. The activity was conducted at Radio Science Laboratory of the Second Faculty of Engineering of the University of Bologna at the Forlì premises under the supervision of Professor Paolo Tortora, Project Manager of the Mercury Orbiter Radio science Experiment (MORE). The experiment is developed as a strict collaboration with the University of Rome 'La Sapienza' and the University of Pisa and the Computer Vision Group of the DEIS department of the University of Bologna.

In particular, the research regarded one of the objectives addressed by the radio science investigations consisting in the retrieval of Mercury's rotational state, that is estimating the obliquity of its spin axis and the amplitude of the librations, oscillations superimposed to the nominal spin rate.

The rotation experiment is accomplished as a jointly interaction among different payloads employing the optical images acquired by the High Resolution Imaging Channel (HRIC) of the SIMBIO-SYS instrument, radio tracking data provided by the Mercury Orbiter Radioscience Experiment (MORE) Ka-band transponder and the Italian Spring Accelerometer (ISA) readings, all part of the Mercury Planetary Orbiter (MPO) scientific payload. For the sake of the experiment an optimal planning of the observations is fundamental to estimate the rotational parameters at the desired accuracy. In order to accomplish this task an end-to-end global simulator was designed and a software for the simulations of the predicted observations, selection and optimization was implemented in the frame of this research activity.

Chapter 2

The BepiColombo mission at Mercury and the Radio Science Experiment

Among the planets of the solar system Mercury is the less explored so a lot is yet to be discovered and explained concerning our innermost planet. Until now, only two NASA's missions flew aiming at the investigation of Mercury, respectively the Mariner 10 probe reaching the planet in 1974 and the MESSENGER spacecraft which was recently inserted in its orbit in March 2011. Other fundamental investigations were performed without the need of sending any spacecraft into space but exploiting the potentialities of Earth-based observations.

Besides, the European Space Agency as well demonstrated the interest in unveiling the secrets of Mercury designing one of the most challenging missions ever, called BepiColombo. The probe is foreseen to reach its destination in 2020 with the launch programmed in 2014 providing the most accurate scientific feedbacks regarding Mercury's study.

2.1 Previous missions and observations

The Mariner 10 flybys performed in 1974-1975 returned the first-ever close-up images of Mercury's surface. In total, three flybys were performed especially thanks to the suggestion by Colombo that observing the orbital periods of the spacecraft and Mercury after the first flyby proposed a gravity correction allowing for a second encounter six months later. The mission provided a 40-45 % global mapping of the surface at the average resolution of about $1 km$/pixel and a few at about $100\, m$/pixel (Murray 1975) via the imaging system, showed the presence of a tenuous atmosphere mainly composed by Helium. Doppler and radio occultation observations also permitted to retrieve its mass of $3.302 \times 10^{23}\, kg$ and mean radius of $2439 \pm 1\, km$ thus leading to the determination of its density (Anderson, et al. 1987). With a value of $5430 \pm 10\, kg/m^{-3}$, Mercury surprisingly revealed to possess the second largest mean density in the solar system while

being the smallest terrestrial planet. If the mean density is comparable with the ones of the Earth and Venus presenting radius sizes twice larger than Mercury, its uncompressed density of $5300\ kg/m^3$ is even more evidence for the existence of larger quantity of heavier elements than the other terrestrial planets (Van Hoolst, et al. 2007). This implies the presence of a large core that could be about ¾ the radius size if mainly composed of iron. However, the most puzzling discovery by the Mariner 10 mission was surely the unveiling of a weak magnetic field approximately 1% that of the Earth supporting a small magnetosphere (Ness, et al. 1974). Other than the Earth, Mercury is unique among terrestrial planets to present this feature. If a dynamo action is the explanation for the creation of the magnetic field this would strongly indicate that a liquid outer core exists together with a solid inner core.

More recently, another NASA mission was developed aiming at the exploration of the innermost planet. After three Mercury's flybys, the MESSENGER spacecraft was finally inserted in a highly elliptical orbit $200 \times 15000\ km$ in March 2011, starting its nominal one year mission. Up to now the dual imaging system composed by a wide and narrow angle camera was able to map almost the entire surface, allowing to capture features at resolutions as small as $18\ m$ (NASA Web site, MESSENGER mission s.d.).

2.2 The BepiColombo mission

The BepiColombo is a cornerstone mission of the European Space Agency (ESA) aiming at the exploration of planet Mercury, the innermost of our solar system. The mission was named in honour of the Italian scientist Giuseppe Colombo, renowned for his several contributions in the field of space missions among which the studies on Mercury and the planification of gravity assists for NASA's Mariner 10 mission.

The BepiColombo mission of the European Space Agency is due for launch in July 2014 and will provide the best understanding of Mercury to date when reaching the planet in 2020 after a cruise phase of about six years (Benkhoff 2011). The mission is jointly developed by ESA and JAXA (Japanese Aerospace Exploration Agency) each agency contributing with a different spacecraft, respectively the Mercury Planetary Orbiter (MPO) and the Mercury Magnetospheric Orbiter (MMO). The MPO is optimized for a global characterization of the planet itself while MMO will focus at the investigation of its environment, especially the exosphere and the magnetosphere. During the cruise phase the spacecraft will make use of a Solar Electric Propulsion Module and perform one gravity assist around the Earth, two around Venus and four at Mercury (Gar09). Chemical propulsion will instead be employed at the injection into orbit. The MMO will first be released into a $400 \times 11824\ km$ orbit and a further thrust manoeuver will then insert MPO into a $400 \times 1508\ km$ orbit, where the spacecrafts will start their one terrestrial year mission.

The scientific objectives addressed by BepiColombo range from the study of its origin and evolution, as well as the determination of its figure, interior structure and dynamics which will be fundamental to explain the origin of its intrinsic magnetic field, studies on the exosphere and

magnetosphere, determination of its composition, and relativity and gravitational physics experiments.

2.3 The Mercury Orbiter Radio science Experiment (MORE)

The research activity presented herein was conducted as a part of a wider project that is the radio science experiment hosted on-board the BepiColombo mission already introduced in the preface to the thesis.

The Mercury Orbiter Radio science Experiment (MORE) is a rather complex experiment and is primarily based on the exploitation of precise microwave tracking of the spacecraft. The employment of the radio link between the Earth and the probe, the usage of dedicated software and the data provided by others on-board instruments are the fundamental tools through which the scientific requirements are met at the desired level of accuracy. Thanks to the implemented technology it is possible to state that BepiColombo is equipped with the most complex and accurate radio system ever flown in a space mission, as will illustrated in section 2.3.2.

2.3.1 Scientific objectives

The Mercury Orbiter Radio science Experiment addresses several scientific objectives varying from investigations on the planet itself, i.e. geodesy and geophysics studies, to experiment in the field of fundamental physics. Radical improvement with respect to the MESSENGER mission and unveiling of the questions arisen by Mariner 10 are foreseen.

Basically, it is possible to identify three major areas of investigation concerning MORE:

- Gravity Field Experiment (Geodesy)
- Rotation Experiment (Geophysics)
- Fundamental Physics

The first objective concerns the estimation of Mercury's gravity field: an estimation of the spherical harmonic coefficients up to degree and order 25 is foreseen, with accuracies that can reach level of 10^{-9}, and Love number k_2 determined with a signal-to-noise ratio of 50. The only data known regarding Mercury gravity field are the estimate of the degree and order two coefficient obtained from the three flybys of Mariner 10 in 1974-75 (Anderson, et al. 1987). Although the principal observations are represented by range and range-rate radiometric observables, the experiment cannot prescind from additional data furnished by other on-board payloads, such as the attitude control subsystems and the accelerometer (ISA). The last in particular provides measurements of non-gravitational accelerations that are crucial for the orbit determination, otherwise seriously comprised. The accuracies needed for the non-gravitational perturbations are of the order of $10^{-6} cm/s^2$. In order to comply with these requirements periodic

calibrations of the accelerometer are necessary to compensate the spurious signals generated by temperature variations.

Orbit determination consists in a procedure which iteratively corrects the model propagating the spacecraft trajectory by a direct comparison of the estimated observables with the real ones. Radiometric observables taken at higher frequencies are desirable since their capability of decreasing the effects of charged particles present in dispersive media leads to better accuracies. The disturbance introduced by coronal plasma is the one most affecting the telecommunication link, especially in correspondence of low Sun-Earth-Probe angles (SEP). MORE foresees to infer the spacecraft position in a Mercury centric frame at accuracies of the order of $10\ cm$ to $1\ m$ (1σ). Accuracies of the order of $1 \mu m/s$ are expected for the S/C velocity.

Precise orbit determination provided by MORE will be beneficial also for the other payloads. Along with guidance purposes, this is a part of the navigation process. In particular, by the synergic combination of precise orbit reconstruction and gravity field information with the measurements collected by the on-board laser altimeter it is possible to define the topography of the planet. A topographical map allows for the definition of a digital terrain model and when removed from gravity field data makes possible to use gravity anomalies information for studies on the sub-surface structure. The BepiColombo Laser Altimeter (BELA) will provide measurement of the distance between the spacecraft and the subprobe point on the surface of Mercury at an accuracy of about $1\ m$. For the horizontal resolution along track a trade-off between the frequency of the observations and the power consumption had to be encountered, resulting in the choice of $10\ Hz$ as baseline (Thomas, et al. 2007). This implies a distance on ground between two following pulses of $258\ m$ at periherm.

The Rotation Experiment has the aim of retrieving Mercury's rotational state. The interest in estimating the obliquity and the librations amplitude of the planet, which characterize its rotational state, lies in the fact that they directly connected to the interior composition of Mercury (Peale, Rotational dynamics of Mercury and the state of its core 1988). A method originally proposed by Peale (Peale, Inferences from the dynamical history of Mercury's rotation 1976) permits to constrain the size and internal state of a planet by measuring the small deviations of the spin rate with respect to its mean value[1,3] The obliquity represents the inclination of the planet's rotation axis with respect to the orbit plane while annual forced librations consist in periodical oscillations around the spin axis superimposed to the nominal rotation rate.

The underlying idea consists in capturing images of the same landmark on the surface of the planet at different epochs in order to observe a relative displacement of the identified features with respect to a uniform rotation. A certain number of observables is obtained and can be fed into an estimation algorithm employing a rotational model which is corrected step by step until rotational parameters are estimated at the desired level of accuracy. In order to accomplish the experiment, MORE avails itself of the fundamental collaboration of another on-board payload, the High Resolution Imaging Channel (HRIC) of the SIMBIO-SYS payload, a camera capturing images at high resolution.

Observations must be planned accurately in order to obtain image pairs carrying the highest information content for the following estimation process. The task is not trivial especially in light of the several constraints involved. First of all, the peculiar Mercury's dynamic characterized by a 3:2 spin orbit resonance and the dependence of librations amplitude on Mercury's mean anomaly leads to the fact that under the same illumination conditions no libration is observed. This places a significant level of difficulty also in the process of images correlation since it will be necessary to deal with high variations in illuminations and scales.

Mercury represents an ideal environment for performing fundamental physics studies. This is due to the fact that relativistic effects are much stronger due to its higher velocity around the Sun compared to the other solar system planets. Among the objectives proposed by MORE in this field is the estimate of the Post Newtonian parameter γ improving the current one by 10 times, determine the gravitational oblateness of the Sun J_2 to better than 10^{-8}, a better definition of upper limits for the time variation of the gravitational constant G (Iess, Asmar e Tortora, MORE: An advanced tracking experiment for the exploration of Mercury with the mission BepiColombo 2009). The estimation of the moment of the solar quadrupole J_2 influences the advance of Mercury's perihelion and is strictly connected to the determination of PN parameters β and γ. Its measurement will be fundamental to obtain further information on the interior of the Sun.

2.3.2 Instrumentation

MORE is a system level experiment whose accomplishment depends not only on its primary payload, the Ka-band transponder (KaT), but also heavily relies on the collaboration of the other subsystems hosted on-board the MPO. High precision radio tracking data provide the fundamental observables, i.e. Doppler and range measurements: the use of a multifrequency X/X, X/Ka and Ka/Ka link allow for an almost complete plasma calibration with the Ka/Ka link being supported by the MORE Ka-band transponder implementing an high precision ranging channel. These data in conjunction with the tri-axial accelerometer (ISA) measurements of large non-gravitational ac-celeration and attitude reconstruction from the ACS subsystem are used to compute the gravity field. Ground station equipment for simultaneous tracking of the three frequency links is also needed along with ancillary equipment for the calibration of tropospheric effects, especially water vapour radiometers for estimating the wet path delay. Moreover, the support from the SIMBIO-SYS team is fundamental since it provides the key observables for the experiment. In fact, images of Mercury collected at different epochs allows to compute the displacement of target points on the surface and thus monitoring the deviations from the predicted rotational model.

On ground	**Ground Station**	Equipped for simultaneous transmission and tracking of the three frequency links X/X, X/Ka, Ka/Ka
	Ground station ancillary equipment	Water vapour radiometer (WVR) for the calibration of wet path delay
On board equipment	**TT&C subsystem**	Includes HGA, RF network, X/X/Ka deep space transponder (DST) providing X/Ka and X/X links. Subsystem used for telemetry and telecommand provided with specific requirements to perform ranging and Doppler measurements with the desired accuracy
	Ka-band transponder (KaT)	Provide the specific radioscience Ka/Ka link for precise Doppler and ranging measurements
	Tri-axial accelerometer (ISA)	Measures non gravitational accelerations
	SIMBIO-SYS	Support from HRIC for the determination of Mercury's rotational state (libration experiment)
	BELA	Support from the on board laser altimeter for the geodesy experiment
	ACS subsystem	Support for attitude reconstruction

Table 1: MORE experiment instrumentation description

As mentioned before, the main observables employed for accomplishing the radio science experiment are represented by range and range rate measurements retrieved from the telecommunication link established between the MPO spacecraft and a ground station on the Earth. Basically, the end-to-end performance of this link is proportional to the accuracy obtained in the measurements. These data will be able to reach an unprecedented level of accuracy in the BepiColombo mission thanks to the exploitation of a multi-frequency link. Two uplink carriers (X and Ka) are sent from the ground station and three downlink carriers (X, Ka1, Ka2) coherently generated from the uplink signal using the Deep Space Transponder and the Ka-band transponder. The three links which are employed for the experiment are summarized in Table 2.

Uplink	Downlink	Transponder
X-band uplink (7.2 GHz)	X-band downlink (8.4 GHz)	DST
X-band uplink (7.2 GHz)	Ka-band downlink (**Ka1,** ~32 GHz)	DST
Ka-band uplink (34 GHz)	Ka-band downlink (**Ka2,** ~32 GHz)	KaT (integrated SSPA Ka-band amplifier)

Table 2: Summary of the multifrequency link used on board the BepiColombo mission

The combined use of X- and Ka-band uplink and downlink communications was first introduced in NASA's Cassini mission (NASA Web Site - Cassini mission s.d.) to Saturn

demonstrating an outstanding impact on the scientific data return of the radio science experiment on-board the spacecraft (B. Bertotti 2003). In fact, thanks to the use of the multifrequency link an almost complete cancellation of the dispersive noises such as solar plasma was possible, thus obtaining precision in the Doppler noise as small as $1\ \mu m/s$.

For this reason, the BepiColombo mission is equipped with a similar system, allowing to separately estimate the uplink and downlink dispersive delay contributions and enabling very precise range and range rate measurements, respectively attaining an and-to-end accuracy of $20\ cm$ at a few seconds integration times and $3\ \mu m/s$ at $1000\ s$ integration time. The ultimate improvement with respect to the Cassini spacecraft is given by the presence of a Ka/Ka band transponder (KaT), representing the MORE payload, which is expressly designed for enabling high phase coherence between the carriers (uplink and downlink) and implements a Wide Band Ranging System (WBRS) for high precision measurements in the Ka-Ka band link. In this way the preferred link for radio science is obtained, the so called Ka2 link, particularly suitable since its higher carrier frequency makes the link almost insensitive to plasma noise. This architecture is used in conjunction with the other two links X/X and X/Ka for which the Deep Space Transponder (DST) already part of MPO's TT&C equipment is used. While DST carriers are phase modulated by a PN ranging code at 3 Mcps, the Ka2 link implements a WBRS employing a regenerative PN ranging scheme which is essential for fundamental physics investigations.

This configuration makes the BepiColombo telecommunication system the most complex one ever conceived flying on a space mission. Such an advanced system is fundamental for the success of experiments conducted in the Mercury's environment, so close to the Sun and dominated by solar plasma delays, especially in light of the relativity experiments foreseen during the conjunctions and the study of the solar corona.

Obviously, the experiment not only relies on the performances of a flight hardware but also on the ground station equipment that is the antenna on the Earth receiving the signal from the spacecraft. Nowadays, the only station able to operate the uplink in the Ka-band is NASA's DSN Deep Space Station 25 (DSS-25), characterized by a 34 meters antenna and located at Goldstone, California. Although the employment of DSS-25 represents the baseline for the MORE experiment since it is the only one supporting the triple link, the tracking data taken from one of the stations of the European Space Agency are also envisaged to be used for radio science, contributing with additional data to the experiment. The Cebreros ground station is the newest of the ESTRACK complex (ESA's tracking station network) classified as Deep Space Antenna 2 (DSA-2) and located close to Madrid in Spain (ESA Web Site - Cebreros Station http://www.esa.int/esaMI/Operations/SEMVSDSMTWE_0.html). The antenna is composed by a $35\ m$ dish able to operate both in transmission and reception in the X-band, while at the moment is only equipped for reception concerning the Ka-band.

(a) **(b)**

Figure 1:Ground stations used for the BepiColombo experiment
(a) Cebreros Ground Station part of the ESA/ESTRACK complex; the station is characterized by a 35 m antenna dish is able to operate in the X-band (reception and transmission) and Ka-band (reception only); (b) NASA's DSS-25 at Goldstone, the only antenna worldwide able to operate the Ka-band uplink

As already stated in the previous paragraph, the employment of a multifrequency link is a fundamental breakthrough for removing the plasma noise in the observables. Besides, this is not the unique disturbance source present in a telecommunication signal. Basically, the transmission media influencing a signal received from a spacecraft are individuated in solar plasma, ionosphere and troposphere, respectively classified as dispersive media (plasma and ionosphere) and non-dispersive (troposphere). Provided that tracking noises caused by media such as plasma and ionosphere can be successfully compensated thanks to the combined use of different telecommunication links, the delay due to Earth troposphere remains one of the error more affecting the observable. The tropospheric delay is essentially composed of two contributions, the so called dry and a wet path delay. While the first one can be easily modeled the same is not valid for the wet component, more difficult to estimate although its smaller contribution.

For this reason, microwave radiometers (WVR) capable of estimating the wet path delay due to the Earth troposphere are installed as ground station ancillary equipment. Usually, the interferences caused by Earth atmosphere are primarily estimated on the base of meteorological data both from NASA's and ESA's stations. However, ground weather measurements are not sufficient to provide a reliable estimation of the wet path delay due to the poor mixing of water vapour and the large variability of its magnitude, spanning in a range of 5 to $20\ cm$ referring to zenithal elevations.

Moreover, NASA also employs multidirectional, dual frequency GPS measurements collected on ground that unfortunately are inadequate for MORE, which requires a calibration of the absolute path delay of the order of 10% (Team 2009). For this reason the continuous

measurements collected with a Water Vapor Radiometer all over the mission duration are fundamental to achieve the desired precision in the data. Since a long time VLBI has employed WVR reaching accuracies of 10-20% on the total wet delay. Despite that, the need to develop advanced media calibration systems arose for complying with the requirements imposed by the Cassini Gravitational Wave Experiment (Allan deviations $\sim 3 \times 10^{-15} @ 1000\ s$), for which a new class of Advanced Water Vapour Radiometers (AWVR) was built, reaching a 5 % accuracy. MORE requirements are one third less demanding compared to the ones of the Cassini mission since the calibration needed for the wet path delay is of the order of 10%, hence a standard WVR is sufficient. In addition to that ESA ground stations should be equipped with instruments able to measure dry and wet tropospheric path delays at sub-centimeter level. At this scope dual frequency receivers have been installed at the station complexes acquiring GNSS data used to perform calibrations.

Chapter 3

Mercury's dynamics and its planetary environment

In this chapter the aspects relative to the dynamics of Mercury are presented and analyzed. In particular, the Mercury's rotation and revolution around the Sun and the environment of the planet are studied since they represent a key aspect in the frame of the radio science experiment.

3.1 The mission environment

Among the solar system planets Mercury is the closest to the Sun and also the smallest one. This vicinity to our star is responsible for the harsh environment the planet is characterized by, presenting surface temperatures that can vary between $-180°C$ at night and $430°C$ during the day which is one of the reason deterring space missions to visit the planet. In fact, the spacecraft orbiting around Mercury is required to withstand thermal loads in terms of solar radiation flux and Mercury's IR emission that are very severe. The distance from the Sun is sensibly varying during its revolution due to the high eccentricity of the orbit, reaching the closest point at perihelion at a distance of about $46 \times 10^6 km$ up to the $70 \times 10^6 km$ at aphelion, thus determining a variation in the flux density received by the Sun as well. In this cases it is useful to refer to the mean solar. The solar constant is defined as the amount of incoming solar electromagnetic radiation per unit area incident on a plane perpendicular to the rays and its mean value on Mercury is about $9130\ W/m^2$. If one takes into consideration that this value on the Earth is around $1361\ W/m^2$ it is possible to have an idea of how the thermal environment existing on Mercury could be harsh.

As a matter of fact, only two missions have explored the planet so far, NASA's probes Mariner 10 in 1974-75 and MESSENGER, inserted in 2011. In appearance Mercury presents many analogies with the Moon, characterized by a surface heavily cratered alternated with plains. Due to the small obliquity the subsolar point is permanently insisting in the equatorial regions thus determining the existence of areas at the high latitudes never reached by the sunlight, such as the bottom of some craters.

3.2 Orbital dynamics

Mercury is characterized by a singular spin-orbit resonance which is different from the others observed in the planets of the solar system. Before its discovery, it was believed that the rotation period was equal to the revolution time to orbit around the Sun, supporting the 1:1 spin/orbit resonance also observed for the motion of the Moon around the Earth. It was Colombo in 1965 (Colombo, Rotational period of the planet Mercury 1965) who originally proposed that Mercury was following a 3:2 spin-orbit resonance, basing its assertion on the radar observations performed by Pettengill and Dyce at the Arecibo Observatory in Puerto Rico (Pettengill e Dyce 1965). In fact, Mercury performs three rotations around its axis while completing two revolutions around the Sun, with rotation and revolution periods respectively equal to 58.68 and 87.96 days. Such dynamic implies that one Mercury day as a period of 176 Earth days, longer than rotation and revolution ones. A solar day is in fact defined as the amount of time necessary to see the Sun in the same position in the sky taking as observation point a place on the surface of the planet. This event occurs after two revolutions or three rotations of the planet, i.e. three Mercury sidereal days.

Earth-based radar measurements also provided further evidence that Mercury occupies a Cassini state as originally hypothesized by Colombo (Margot, et al. 2007), in which the orientation of its rotation vector is in an equilibrium position. A system is defined to be in a Cassini state if obeying to the three laws established by Cassini in 1963 for describing the motion of the Moon.

For a tidally locked body:

1. Rotation rate and mean orbital rate are synchronous
2. Spin axis as constant inclination with respect to the ecliptic plane
3. Spin axis, orbit normal and ecliptic plane are coplanar

In particular Mercury is thought to occupy a Cassini state 1, a condition in which the rotation axis and the orbit normal are coplanar with the normal to the Laplace plane while the rotation axis of Mercury and the orbit normal are precessing about the normal to the Laplace plane with a period of about $280000\,years$ (Colombo e Shapiro, The rotation of planet Mercury 1966), (Peale, Generalized Cassini's laws 1969). The Laplace plane is defined to be reference plane about whose axis the instantaneous orbital plane of a body precesses. Mercury is thus also in a 1:1 resonance between the secular precession rate of the node of Mercury's equatorial plane with respect to the ecliptic plane and the ascending node of the orbit (Van Hoolst, et al. 2007).

3.3 Librations

Mercury's shape is not perfectly spherical and the contributions determining the mainly deviations are essentially two. The first one is a polar deformation described by the coefficient C_{20} in the spherical harmonics decomposition, estimated to be of the order of 60×10^{-6} (Anderson, et al. 1987), and the equatorial flattening represented by the coefficient C_{22}, estimated to be of the

order of 10×10^{-6} (Anderson, et al. 1987). Mercury is also characterized by the highest eccentricity among the planets of the solar system, with a value of $e \sim 0.206$. This, in conjunction with the large equatorial flattening abovementioned, determines the generation of a Sun forcing torque acting on the bulge of the planet when the longest axis of the equatorial plane is not perfectly aligned to the Sun-Mercury direction, as shown in Figure 2. Basically, this is the mechanism determining the planet's stability of the spin-orbit resonance in a 3:2 configuration instead of a 1:1, and that also is responsible for the arising of the so called annual librations, since they are resulting by the interaction between the Sun and Mercury and the revolution time of the last one gives the period to the librations (=1 Mercury year).

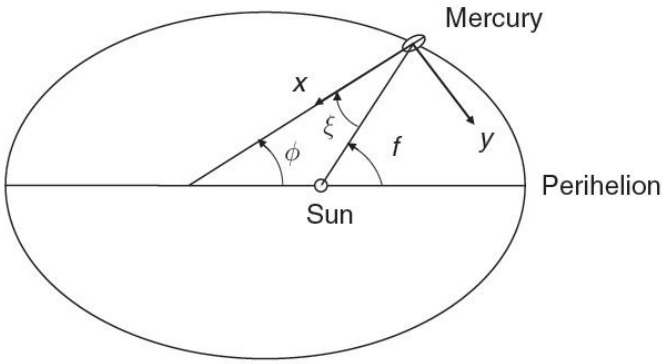

Figure 2: Illustration of Mercury's motion around the Sun.

Due to the high orbit eccentricity, a forcing torque, periodic with the orbital period of Mercury, acts on the equatorial asymmetric bulge of the planet

Librations are oscillations in longitude superimposed to the nominal rotation of the planet and since they are dependent on the solar torque which varies its magnitude according to Mercury's position in its revolution path, it is straightforward that the forced libration presents a period of 88 days. When referring to libration amplitude, one means the maximum value in the longitudinal angular deviation with respect to Mercury's rotation. Librations are normally described as longitudinal since the latitudinal effect due to the obliquity and planetary asymmetries in the North-South pole direction are neglected in this treatise.

The torque exerted by the Sun on Mercury's bulge can be expressed with the following relationship (Pfyffer 2010), (Van Hoolst, The Rotation of the Terrestrial Planets 2007):

$$T = \frac{3}{2}(B - A)\frac{GM_{Sun}}{r^3}\sin 2\xi \tag{3.1}$$

Where A and B are Mercury's principal moments of inertia, r is the distance between the centers of mass of the Sun and Mercury and ξ is the angle between the Sun-Mercury direction and Mercury's axis characterized by the smallest moment of inertia, see Figure 2. From the figure it also possible to derive the angle of rotation of the crust, which is the one visible from the outside, and

corresponds to the difference between the true anomaly of the planet f and the angle ϕ defined by the intersection of Mercury's axis with the smallest moment of inertia and its orbit major axis:

$$\xi = f - \phi \tag{3.2}$$

The torque can be considered to assume the following expression if the mantle alone is determining the equatorial asymmetry $(B - A)$ and if its libration is decoupled by the core:

$$C_m \ddot{\xi} = T \tag{3.3}$$

Where C_m is the moment of inertia of the mantle. From the knowledge of Mercury's 3:2 spin-orbit resonance it is possible to describe the libration angle with the following:

$$\lambda = \xi - \frac{3}{2} MA \tag{3.4}$$

Where MA denotes Mercury's mean anomaly. Substituting equation 3.4 in 3.3 one obtains:

$$C_m \ddot{\xi} = C_m \ddot{\lambda} \tag{3.5}$$

Hence, it is possible to rewrite equation 1 inserting the libration angle λ:

$$\ddot{\lambda} = -\frac{3}{2}\left(\frac{B - A}{C_m}\right)\frac{GM_{Sun}}{r^3}\sin(2\xi - 2f + 3MA) \tag{3.6}$$

As it will be explained later in a more detailed way, librations can be a significant instrument for deriving information on the interior structure of Mercury, still undetermined. The physical librations phenomena can be divided into two categories: 'forced libration', the one deriving from the mechanism abovementioned, and 'free libration', both connected to the mantle moment of inertia. Free librations depends on the frequency of the eigenmode of the system formed by the Sun and the planet into consideration, which is strictly connected to the shape of the planet (Pfyffer 2010).

Other planetary librations exist, whose mechanism is analogous to the one exerted by the Sun gravity torque. In this case as well they can be modeled with a period coinciding with the one of the perturbing force.

3.4 Mercury's interior

One of the reasons why Mercury has gathered the attention of the scientific community is the surprising revelation of the existence of a dipolar magnetic field on the planet, discovery made

during the Mariner 10 flybys. The probe measured an intrinsic global magnetic field generating a small magnetosphere bounded by a magnetopause and detected a tenuous atmosphere (Milillo e et al. 2010). The extent of the magnetic field has been estimated to be of the order of 1% the one of the Earth. Different explanations arose to explain the observation. The preferred one is existence of a dynamo effect generated by the presence of a liquid outer core decoupling the dynamic of the external layers and the interior core, while other interpretations propose a residual magnetism in the crust and a solid core. The second one better fits with the evidence of a mean high uncompressed density bearing on a core made of pure iron. On the contrary, recent Earth-based observations indicates that the core is at least partially molten (Margot, et al. 2007). The study of the internal structure of Mercury is one of the objectives of the rotation experiment part of MORE.

In fact, so far models of the interior of Mercury relied on the measurement of its uncompressed density. In Figure 3 a plot radius-density of the terrestrial planets is shown.

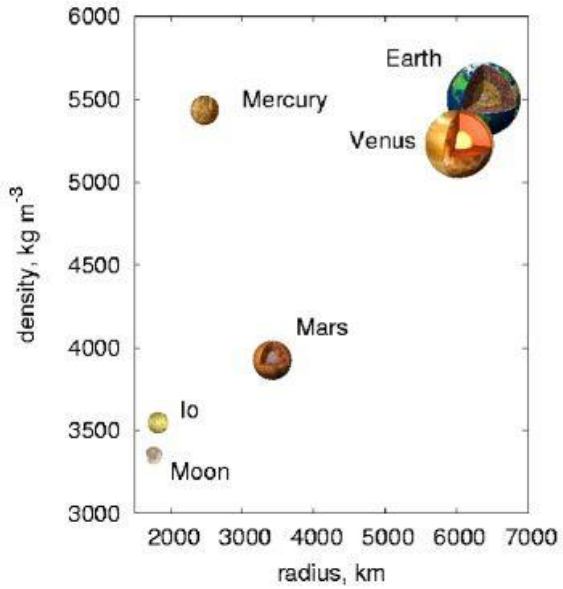

Figure 3: Terrestrial planets, Moon and Jovian satellite Io densities with respect to the radius

Compared to gas giant planets of the outer solar system, terrestrial planets are characterized by low masses, small radii, and large densities. Their chemical compositions is rich in rock-forming elements and metals such as iron and nickel, the latter concentrated in central cores. Interiors are usually strongly differentiated and subdivided like that of the Earth into a partly or entirely liquid metallic core, a silicate mantle and an outermost crust derived from partial melt processes of the underlying mantle. When observing Figure 3 it is self-evident that Mercury presents a value of density significantly higher compared to the Earth, Venus and Mars. This is a demonstration of a larger presence of heavier elements and is evidence for the presence of a large core mainly composed by iron.

Still, the composition and the structure of the interior of Mercury remains to be defined. It was originally proposed by Peale an effective method for constraining the size and internal state of a planet by measuring the small deviations of the spin rate with respect to its mean value (Peale, Inferences from the dynamical history of Mercury's rotation 1976), (Peale, Rotational dynamics of Mercury and the state of its core 1988).

In particular establishing whether Mercury's core is molten or solid is of particular interest. The presence of a liquid core would reflect in observing a libration amplitude twice larger than if a completely solid core existed. The method is based on the combined knowledge of the libration amplitude, the obliquity, and the second degree and order gravitational harmonic coefficients C_{20} and C_{22}.

Assuming that the core presents a libration differing from the 88-day of the entire planet and the core is not following the mantle on the timescale of spin precession which is of the order of 250000 years, the ratio between the mantle-crust moment of inertia C_m and the one of the entire planet C is given by:

$$\frac{C_m}{C} = \left(\frac{C_m}{B-A}\right)\left(\frac{B-A}{MR^2}\right)\left(\frac{MR^2}{C}\right) \leq 1 \tag{3.7}$$

Where $A < B < C$ are Mercury's principal moments of inertia, with M and R being its mass and radius respectively. The first factor of Eq. 3.7 can be derived from the forced libration amplitude ϕ since the following relationship exists:

$$\phi \propto \left(\frac{B-A}{C_m}\right) \tag{3.8}$$

The second term is four times the harmonic gravitational coefficient C_{22} while the last one satisfies the Cassini state equilibrium for the obliquity of the rotation axis. A strong coupling between the core and the external layers results in a C_m/C value equal to 1 while values closer to 0.5 would be evidence for at least part of the core to be fluid.

Chapter 4

MORE Rotation Experiment

This section covers the practical aspects of the MORE rotation experiment, whose objectives consists in the retrieval of Mercury's rotational parameters. The scopes are analyzed in detail especially concerning their relevance in the frame of Mercury's exploration, still presenting many questions to be explained. The observational strategy of the experiment is illustrated and the architecture of the global end-to-end software implemented for simulating the experiment is presented.

4.1 Rotation experiment overview

The Mercury rotation experiment addresses the retrieval of Mercury's rotational state. In fact, from the knowledge of the obliquity and the librations amplitude of the planet, which characterize its rotational state, it is possible to derive information on the interior composition of the planet as proposed by Peale (Peale, Inferences from the dynamical history of Mercury's rotation 1976), (Peale, Rotational dynamics of Mercury and the state of its core 1988).

The obliquity represents the inclination of the planet's rotation axis with respect to the orbit plane while annual forced librations consist in periodical oscillations around the spin axis superimposed to the nominal rotation rate. The variation of the librations in time take the form of a sinusoidal wave with a maximum amplitude of 400 m at the equator. Being this phenomenon essentially visible in longitude, obviously the magnitude of the oscillations is decreasing towards the higher latitudes until it becomes undetectable close to the pole (due to the very small value of the obliquity currently estimated to be around 2.11 $arcmin$). This behavior is determined by the gravity torque exerted by the Sun on Mercury's equatorial asymmetric bulge due to the high eccentricity of its orbit.

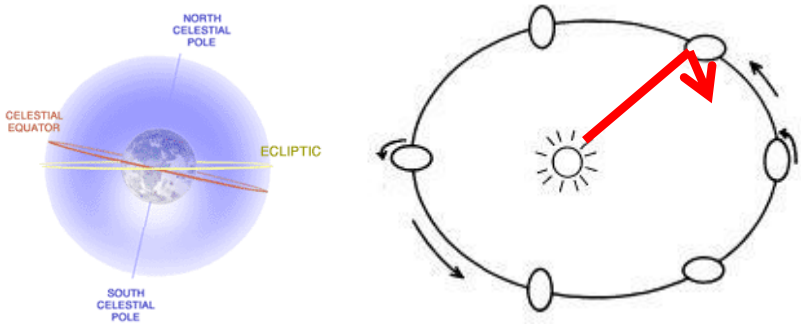

Figure 4: Graphical representation of Mercury's obliquity and librations

As already discussed in the previous section the determination of the rotational state would permit to constrain Mercury's interior, which is still an open issue. The internal structure of the planet, in particular the size and the physical state of the core, can be determined starting from the data on the rotation state and the long wavelength gravity field. Medium length gravity field is instead employed for gathering information on the structure of the mantle and the mantle-core interface, where "mascons" such as the ones existing on the Moon could be detected. Finally, external layers such as the crust and the crust-mantle interface are studied on the base of altimetry observations and the gravity field estimated thanks to the orbit determination process.

Current rotational state estimate		
	Estimate	**Accuracy**
Obliquity	2.11 arcmin	0.1 arcmin
Libration amplitude	35.8 arcsec	2 arcsec

Table 3: Current best estimate of Mercury's rotational parameters, obliquity and librations amplitude, obtained by means of Earth observations (Margot, et al. 2007)

The scope of the experiment is to improve the current estimate of rotational parameters (accuracy of 0.1 $arcmin$ for the obliquity and 2 $arcsec$ for librations) to a precision of the order of 1 arcsec for both obliquity and librations amplitude ($12\,m$ on the surface). The harmonic coefficients of degree-two C_{20} and C_{22} will instead be determined by the gravity field experiment at a level of accuracy of 10^{-9}1-sigma.

Among the experiment envisaged by radio science this is probably the one requiring the interaction between the different subsystems hosted onboard the S/C. The telecommunication link, tri-axial accelerometer measurements of non-gravitational acceleration and attitude reconstruction from the ACS subsystem are used for precise orbit determination. Moreover, the support from the SIMBIO-SYS team is fundamental since it provides the key observables for the experiment. In fact, images of Mercury collected at different epochs allows to compute the displacement of target points on the surface and thus monitoring the deviations from the predicted rotational model.

The process of image pairs selection is then a critical issue to the observations planning as it should satisfy science operations constraints as well as optimizing the pattern matching and estimation procedures. Above all, only a limited number of observations will be available to the MORE team thus further stressing the importance of accurately planning the observations. In the frame of this study, innovative observational strategies are being considered in the selection process that could strongly influence the relaxation of some of the imposed constraints, such as super-resolution acquisitions, allowing the enhancement of the original resolution up to four times, and the use of ad-hoc pattern matching algorithms more robust to illuminations and scales variations.

The purpose of the research activity is driving the selection process of optimal surface coordinates selection. At this scope, it was decided that the better solution was undertaking a simulation of the experiment implementing an end-to-end global simulator taking as the starting point the database of the observations really feasible during the duration of the mission and returning as output the more convenient features and epochs of observation in terms of best scientific result.

4.2 Observational strategy

The rotation experiment strategy consists in collecting images of the same landmarks on Mercury's surface taken at different epochs by means of the high resolution camera (HRIC) part of the SIMBIO-SYS payload, as shown in **Errore. L'origine riferimento non è stata trovata.**. By capturing the same feature on the surface in two distinct times allows to observe how the planet has moved in the time interval and thus information on the rotational state are contained in the images. In particular, it is possible to compare the displacement effectively observed from the real images to the one expected from the rotational model used to simulate Mercury's dynamics. It is this disagreement between the 'observed observable' and the 'simulated observable' that permits to adjust the rotational model until convergence, thus determining the desired obliquity and libration.

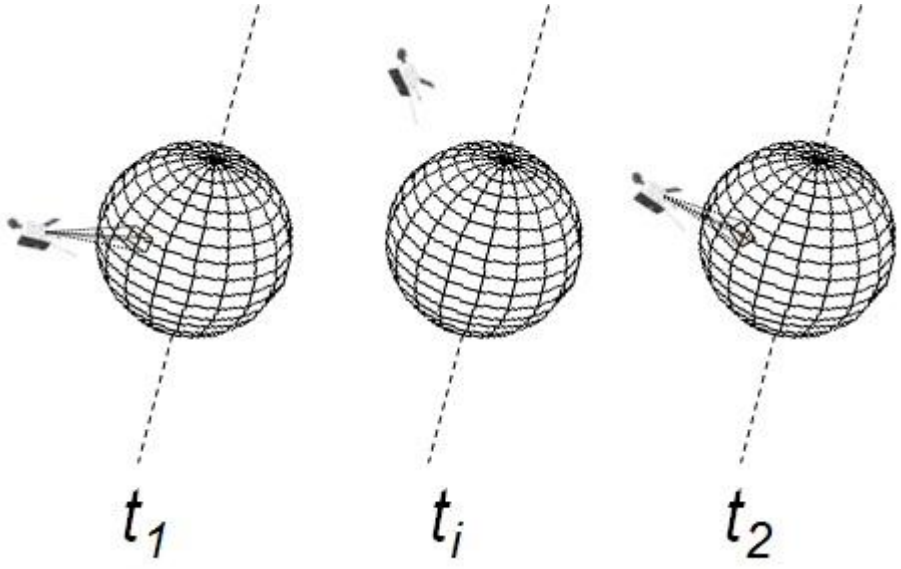

Figure 5:Observational strategy of the rotation experiment
The technique at the base of the rotation experiment consists in capturing images via the high resolution channel of the of same region on Mercury's surface taken at two different epochs. The displacement of selected tiepoints in the two images is computed by means of ad-hoc pattern matching algorithms and represents the observable used as input for the estimation software

Practically, this process is made executing an image correlation between the images depicting the same landmark, procedure which is carried out applying dedicated pattern matching procedures first identifying the notable features in the images and then correlating them, as shown in a simplified example in Figure 6. Hence, the relative displacement of the selected target points in the two acquisitions are computed, referenced in an inertial frame. As already mentioned, the computed displacements represent a direct observable of the evolution of Mercury's rotation in time and are used as inputs to feed into an estimation software iteratively adjusting the rotational model until convergence is met.

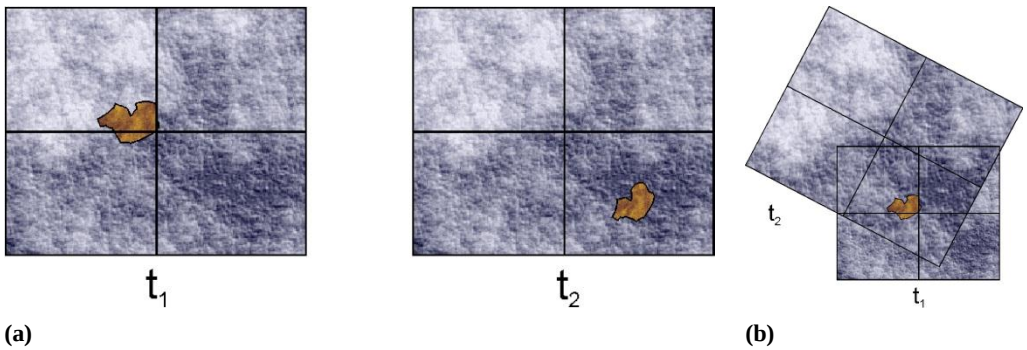

Figure 6: Simplified graphical example of the pattern matching process between two images relative to the same area of Mercury's surface
first the landmark is detected in both the images (a), successively a correlation process takes place where the displacement of the selected features are determined (b) (Iess, Mercolino, et al. 2003)

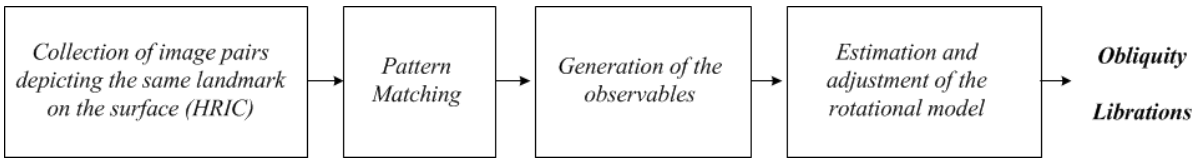

Figure 7: Flow chart summarizing the procedure employed for the realization of the MORE rotation experiment

One of the major issues in the rotation experiment planning is the determination of the most suitable features to be observed on the surface, problem which is strictly connected to the pattern matching strategy following selected, and also the determination of the most favourable epochs for the observations, this parameter also influenced in some way by the image correlation algorithms.

Even performing a preliminary analysis of the problem, before any process of optimization necessary for refining and searching for the best observational strategy, the study of Mercury's dynamics provides significant information in this way. In fact, the planet's 3:2 spin orbit resonance is one of the constraints coming into play, whose effect is clearly evident when looking at Figure 8, presented in paper by Milani et al. (Milani, et al. 2001). In fact, if the phase of the rotation of Mercury and the mean anomaly of its orbital motion taken in an inertial reference frame, respectively the dotted and solid lines, are plotted together, it can be easily noted a resonance of one Mercury day between the two. This means that each two revolutions and three rotation of the planet they both repeat the same configuration. Since the experiment is carried out thanks to the collection of images of the surface, a fundamental parameter to be visualized is given by the illumination conditions on the surface, which depends on the difference between the rotation angle and the true anomaly (curved line). The last could be quite different from the mean anomaly due to the large eccentricity of Mercury' orbit. What is important to extrapolate from this study is the opportunity of flying over the same landmark under good conditions. Since the orbit of BepiColombo is essentially polar, the spacecraft visibility can be represented with two horizontal lines at a distance of 180°, whose intersections with the lines representing the illumination conditions provides the opportunities of observations. Among the 12 possibilities occurring during one nominal mission year only half of them are potentially available since the others corresponds to passages on regions which are in shadow, therefore no useful image could be captured. As the entire dynamic present a resonance period of one Mercury day, the 6 usable opportunities are in effect 3 repeated twice. In order to determine the favourable situations for the estimation of the rotational parameters, it is important to underlie that librations possess a period of 88 days and depend on the true anomaly. Hence, observations taken at time intervals of 176 days present no information content from this point of view thus preventing from distinguishing any oscillation in longitude. The conclusion is that librations phenomena are impossible to be observed under similar illumination condition.

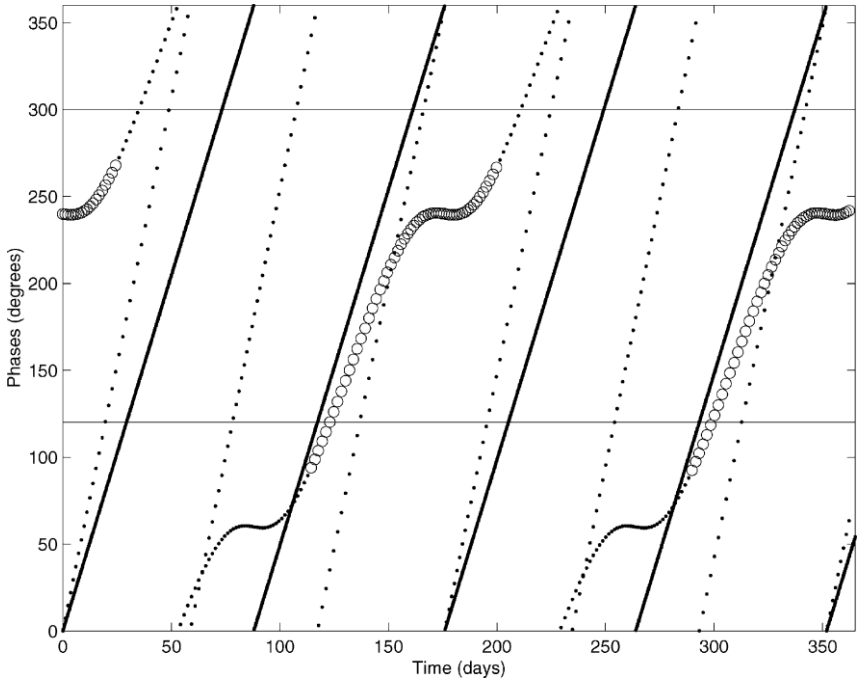

Figure 8: Plot illustrating the opportunities of flying over the same spot on the surface during the BepiColombo mission.
The lines represent the rotation phase of Mercury (slanted dotted), the mean anomaly of Mercury (slanted solid), while the last one represent the visibility conditions in terms of illuminations at a reference longitude; the small circles stand for a shadowed area

This represents an important information as from the very beginning it poses the attention on the issue of implementing pattern matching algorithm particularly robust to the variations in illumination conditions between the images to be compared.

In other studies performed on the feasibility of the rotation experiment and determination of plausible science planning scenarios several constraints were commonly applied to the database of the possible observations. The limitations mainly concerned the illumination conditions at which the images were captured, where extreme configurations of the Sun incidence on the surface were discarded, in order to avoid grazing light and angles too close to zenith. This data were based on a dedicated study (Jorda e Thomas 2000) aimed at providing results on the feasibility of the rotation experiment and selection of the most suitable features on the base of the existing pattern matching techniques.

Further studies performed by the CVG team working at the DEIS department of the University of Bologna which is strictly collaborating with the MORE team demonstrate that modern pattern matching techniques are able to overcome the limitations normally imposed. This result represents an important breakthrough since it enlarges the field of the possible options for the accomplishment of the mission. This would permit to maintain some solutions that might significantly contribute thanks to their valuable informative content. In a same fashion, images taken at the highest altitudes were rejected since characterized by lower resolutions as well as image pairs marked by high changes of scales could be problematic to be treated. Both these

problems were again undertaken demonstrating that the possibility exist to employ even images captured in this conditions.

4.3 Global simulator of the experiment

As already mentioned in the previous section the problem of finding an optimal science observations planning for the rotation experiment is not a trivial task. Mercury's dynamics and illumination conditions creating the proper opportunities for collecting useful data must be taken into consideration. The real obstacle is imposed by the limitation in the number of observables that most likely will be collected. For this reason the selection process assumes such a significant importance: from a proper observational strategy depends the good outcome of the experiment.

Due to the several factors coming into play, it was decided that the best way to reach an exhaustive result was the possibility to reproduce the real execution of the experiment by designing and implementing an end-to-end simulator.

The design flowchart of the simulator underwent different modifications during the research project until it evolved to the more recent stage which is depicted in Figure 9.

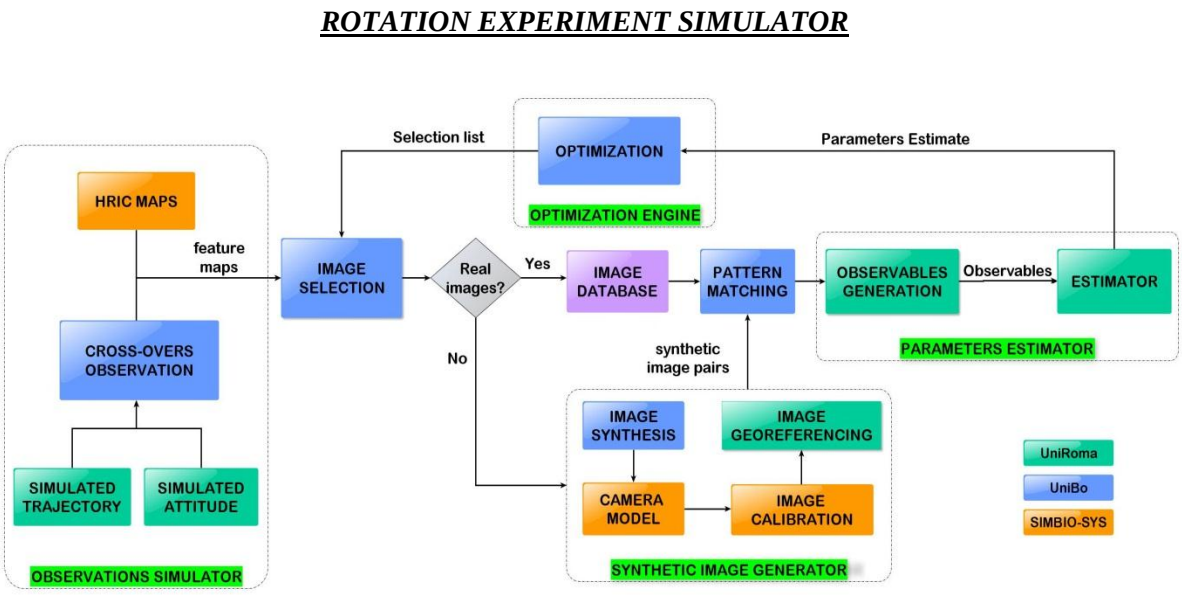

Figure 9: An end-to-end global simulator of the rotation experiment

A global simulator of the entire experiment was designed with the final aim of identifying a science observations scenario optimizing the estimation of Mercury's rotational parameters

The simulator can be substantially divided into four main modules:

- Observations simulator
- Synthetic image generator
- Parameters estimator
- Optimization engine

The observations simulator is the starting point of the entire software providing a database of the possible observations on the surface of Mercury. In this part, the input is furnished by the kernel of the BepiColombo trajectory developed by the UniRoma team and containing the simulated trajectory and attitude. The main routine of the module is the 'cross-overs observation' software. In this program the surface of Mercury represented as a Mercatore map is divided into a cell grid where the center of each cell is represented by a node referred as latitude and longitude. Hence, the representation of the surface is translated into a matrix which is used to reference the passages of BepiColombo on a determined area.

For the duration of the mission at each selected epoch the state vector of the probe is retrieved and the correspondent sup-probe point is identified. The ground area seen by the camera is then computed and the passage on the region captured by the frame is registered in the nodes of the matrix. A database is then created collecting all the information relative to the specific flying over that are useful for successive post-processing.

The first output that is possible to appreciate is a map with a number of passages on the regions of the surface: this provides an immediate idea where the possibility of collecting images is more numerous. However, the HRIC team does not foresee to cover the entire surface of Mercury and it is not sure that the whole set of images which are optimal for the rotation experiment can be requested. For this reason the software also foresees the eventuality of comparing the MORE maps with the ones contemplated by SIMBIO-SYS.

Once that a database of the observations has been generated, these data become the input to the selection software. Starting from the single observations the possible image pairs are computed. As already explained, the observable in this case is in fact provided by the correlation between two frames of the same region taken in different epochs.

An additional database of image couples in terms of coordinates on the surface is then created. In order to select only pairs satisfying certain requisites, some constraints in terms of illumination conditions, altitude or detectable libration might be imposed to filter the results. Among the several possibilities a certain set is then chosen following used for the estimation process.

The flowchart is now forked off into two different options depending on the availability of real images coming directly from the mission or in case synthetic images need to be generated. The second option is fundamental during the pre-mission phase in order to provide images that could be used in the simulator for computing the pattern matching error and generating the observables for the estimation procedure. As explained extensively in paragraph 0, at this aim a collaboration with

the CVG team expert in the field of images elaboration was established. The module concerning the image synthetis comprehends different steps. At the moment a Digital Elevation Module has been implemented that will be in the future updated with the real model of HRIC in order to take into account lenses distortions. Successively the image will be calibrated and georeferenced before its passage to the pattern matching.

At this point images are correlated and the information relative to the pattern matching error is passed along to the estimation module. This block is part of the competences of the University of Roma where a software for the estimation of the rotational parameters has been developed. Before this phase takes place the observables according to the Mercury rotational model at disposal are generated and become the inputs to the software.

Now, the most critical part of the simulator takes place, where starting from the accuracy obtained by the estimator, a new set of observations on the surface of Mercury is selected for the next iteration. This procedure is accomplished by means of an optimization algorithm which adjusts the current planning of observations to a new one supposed to return an improved scientific output. The loop is iterated until convergence to an optimal solution that obviously should comply with the requisites of the mission in terms retrieved accuracy for the rotational parameters.

Obviously, the entire implementation and testing of the global simulator is not trivial and also involves the collaboration among different teams which could sometimes represent a time-consuming activity aimed at coordinating the effort of the groups.

At the time being not all the submodules depicted in Figure 9 are completed yet, and it is very likely that the architecture of the simulator will experience further refinements as the implementation proceeds.

Besides, the resolution at the base of the research activity does not claim to reach a definitive configuration and results in such a short time, all the more that the scientific planning of the rotation experiment also changes with the mission evolution and updates. The software always needs to be elastic with respect to potential rescheduling of mission priorities and variations. To put it in practice, the scientific results that will be the output of the MESSENGER mission currently orbiting around Mercury could be decisive since providing valuable information regarding the unknown gravity field of the planet. This data are fundamental in order to be able to foresee the evolution of the BepiColombo trajectory and in case of dramatic changes in its orbit some actions would need to be taken even leading to variations in the parameters insertion orbit.

Instead, the effort was directed in the sense of designing a preliminary version of the global simulator so as to make available an instrument that could be used to perform preliminary analyses and to be refined and completed in the future. Some of the blocks have already been finalized and tested, such as the observations and selection blocks. As explained before the image processing block is still in phase of development but can be easily bypassed at the moment without hampering the implementation and usage of the other modules. The estimation module developed by the UniRoma team is almost finished as well.

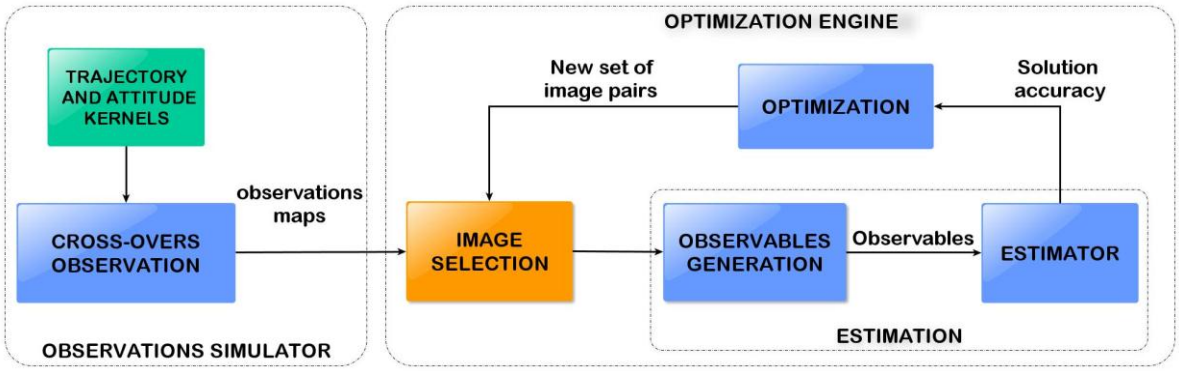

Figure 10: Current state-of-art in the implementation of the global simulator

Due to the complexity and the time required for accomplishing the implementation of the end-to-end simulator, a preliminary version has been implemented. Momentarily, the part relative to the elaboration of the images is bypassed and the pattern matching error is conservatively introduced inside the generation of the observables procedure.

The part which at the moment is at its more primordial stage is certainly the optimization procedure. To accomplish this task a genetic algorithm has been preferred since deemed to be the more suitable for finding the global optimum in the vast space domain of all the possible crossovers. Due to the momentary unavailability of the finalized estimation software and in order to initially simplify the first simulations of the algorithm, a simple software for the estimation of the librations and obliquity of Mercury was implemented. The aim is not substituting the more complex one but build a convenient routine that could be easily integrated in the first release of the optimization module. This facilitates the initial phase of debugging and could rapidly provide information on the efficacy of the chosen algorithm as well as preliminary results regarding the areas where the final solution is more likely to fall in. In fact, the employment of a more simple model for the estimation, although not as precise and well defined such the final version that will be introduced, should be able anyway to provide solutions with a physical meaning that could help for the future iterations and drive the implementation of the optimization software. The architecture of the current state-of-the-art of the software is illustrated in Figure 10.

Chapter 5

Observations simulator

The implementation of the observation module is the initial step from which the simulation of the rotation experiment begins. In order to allow the following processes of estimation and optimization a selection of a set of image pairs needs to be done. For this reason it is necessary to have a database of the crossovers on the surface of Mercury, so that at each iteration it is possible to pick among the possible solutions. Moreover, it is useful that the database also contains the information relative to the passages as they will be used for the generation of synthetic images (illumination conditions and altitude), estimate the visible libration in an image pair (Mercury mean anomaly) and generate the observables (coordinates of the feature on the surface).

The primary output provided by the software is a graphical representation of the observations which is obtained by the computation of the ground tracks of the probe on the surface displayed as a Mercatore map. This gives immediately an idea of the regions that will be mostly covered. In fact, the location of the observations is decisive for the estimation of the rotational parameters. In general, libration motions are higher the more the observed latitude is close to the equator while the obliquity is better estimated at the poles. However, since the estimation accuracy is highly dependent on the number and type of parameters to be included in the process at this moment it is not possible to surely state which could be the preferred observations location on the surface only from the study of Mercury's dynamic. Furthermore, also the conditions at which the images are taken are influent: some images could present a very high informative content but being totally untreatable even with the more advanced pattern matching method.

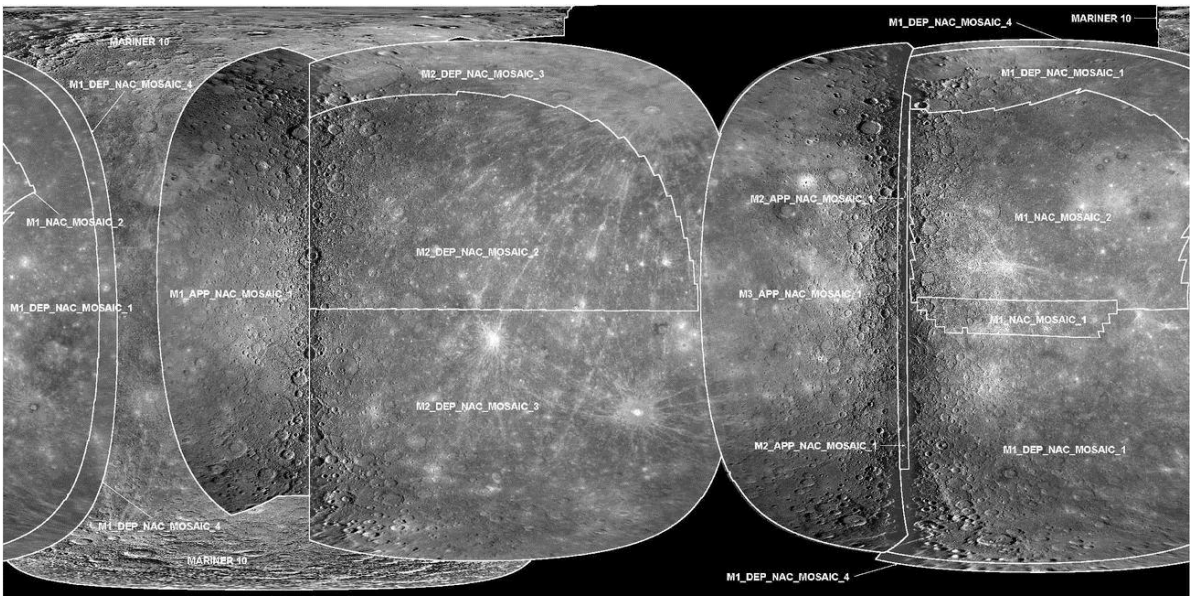

Figure 11: Mercury's surface displayed on a Mercatore map

The images collected by NASA's missions Mariner 10 and MESSENGER have been used to compose like a puzzle the surface of Mercury. The image is reported to make clearer how the surface is conceived to display the observations

5.1 Software description

The software has been entirely programmed in Fortran 90 language and fundamentally consists of two routines. In the first one all the input parameters and simulation settings are defined: global variables, kernels to be used, duration of the simulation, definition of the output folders. The second one is the core software were all the computations are made and final outputs and database saved. The breakdown structure of the core software is shown in Figure 12.

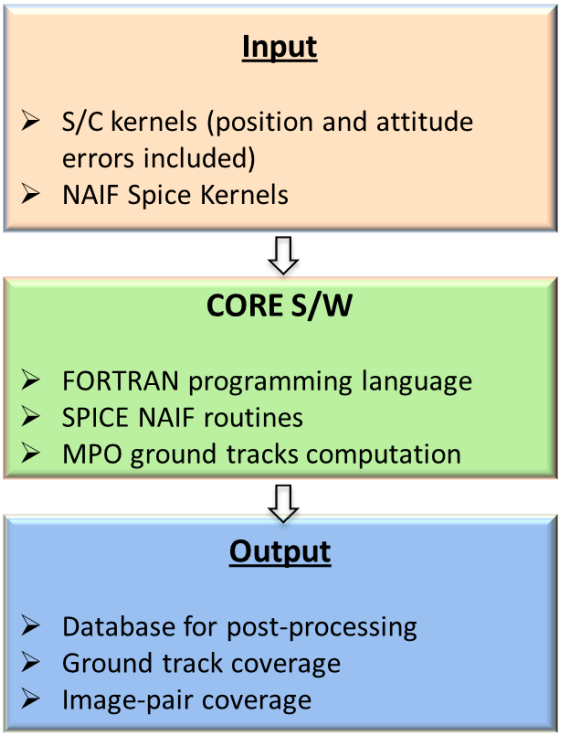

Figure 12: Architecture of the observations software

The architecture of the software is here divided into three main blocks, although the last one formally speaking is in reality included in the core routine. The first phase consists in providing the links to the kernels to be used

5.1.1 Mission scenario and rotation experiment overview

Spice Kernels from NASA's Navigation and Ancillary Information Facility (NAIF) are used for Mercury and the Sun while for the MPO trajectory the kernels developed by the UniRoma team were employed. The kernels were computed using the data from previous MESSENGER flybys for the lowest spherical harmonics and applying Kaula's rule from degree 4 to 30 with $A_k = 9$, without including maneuvers and periodic accelerations.

The BepiColombo orbital elements at the insertion in Mercury's orbit are summarized in Table 4 as released in a report by the Mission Analysis section of ESA/ESOC (European Space Operation Centre). All the simulations have been made considering the last updates from ESAC (European Space Astronomy Centre) which took as baseline for the mission an insertion in the orbit on January 22nd 2021 and the beginning of the science experiments after a commissioning phase lasting one month. As a duration of the mission the nominal one equal to one terrestrial year was taken into account. As it is possible to notice in Table 4, two different scenarios were envisaged for the capture in the Mercurian orbit, where the argument of the ascending node and the argument of pericenter are different depending on a North pole or a South pole approach. The two options refer to a prograde or retrograde orbit although the orbital elements are the same. The

kernels used for simulating the MPO trajectory were developed according to a North pole approach and consequently the computation of the observations as well.

BepiColombo Trajectory data	
Pericentre	400 km
Apocentre	1508 km
Semi-major Axis	3394 km
Eccentricity	0.163
Period	2.325 h
Inclination	90.0°
RAAN	-112.3°(N) 16° (S)
Argument of pericenter	-164.0° (N) 67.7°(S)
Beta angle	0°
(N) considering a North pole approach for the insertion orbit (S) considering a South pole approach for the insertion orbit	

Table 4: Initial orbital elements of MPO in the Mercury equatorial system at the insertion date of 14 September 2019, 9.29 UT. (Garcia, et al. April 2010)

Looking at Table 4, it is clear from the inclination that the probe will perform a polar orbit, characterized by a low eccentricity and a period of two hours and a half. Obviously, this choice is particularly adapt for having the possibility of covering the majority of Mercury's surface and provide a detailed mapping, also favored by the low altitude.

The beta angle is defined as the angle between the Sun-planet direction and the orbit plane, as illustrated in Figure 13.

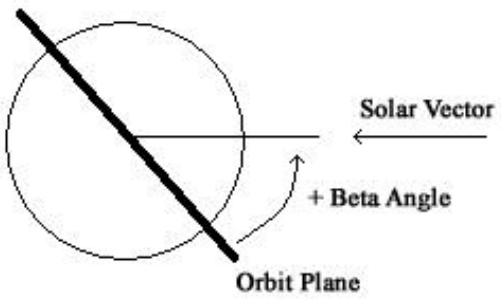

Figure 13: Illustration of the Beta angle

The images of the surface used for the rotation experiment are taken by means of one of cameras part of the SIMBIO-SYS payload, the High Resolution Imaging Channel. The aim of the

SIMBIO-SYS investigation is to provide an extensive coverage of the planet, aim which is nevertheless favored by the design of the BepiColombo trajectory.

Camera	Objectives	Performances
High Resolution Imaging Channel (HRIC)	• Mapping at high resolution with color capabilities	Spatial Resolution: 5 m/pixel @ periherm 19 m/pixel @ apoherm
Stereo and Colour Imaging Channel (STC)	• Global surface mapping with colour capabilities • Global stereo mapping and Digital Terrain Model reconstruction	Spatial Resolution: 50 m/pixel average for images
Visible and near-infrared hyperspectral imaging channel (VIHI)	• Mineralogical mapping • Identification and distribution of mineral species	Spectral range: 400-2000 nm

Table 5: Illustration of the cameras composing the SIMBIO-SYS payload (Flamini e et al. 2010)

The SIMBIO-SYS payload includes imaging systems with stereo (STC) and high spatial resolution (HRIC) capabilities along with a hyperspectral imager (VIHI) in the visible-near-infrared range.

In Table 5 the characteristics of the payload are depicted specifying the performances of the cameras composing SIMBIO-SYS: the High resolution Imaging Channel (HRIC), the Stereo and Colour Imaging Channel (STC) and the Visible and near-infrared hyperspectral imaging channel (VIHI).

The HRIC will provide images at resolutions as high as 5 m/pixel at periherm and 19 m/pixel at apoherm in different bands of the visible. The coverage of Mercury's surface is estimated to be around 20%. The camera design permits to obtain high spatial resolution images over the entire field of view in a panchromatic filter and in three band-pass filters centered at 550, 750 and 880 nm. The Field of View of the camera is 1.47° and the sensor is 2048x2048 SiPIN Complementary Metal Oxide Semiconductor (CMOS) with a pixel size of 10 μm. An image of the SIMBIO-SYS payload is displayed in Figure 14.

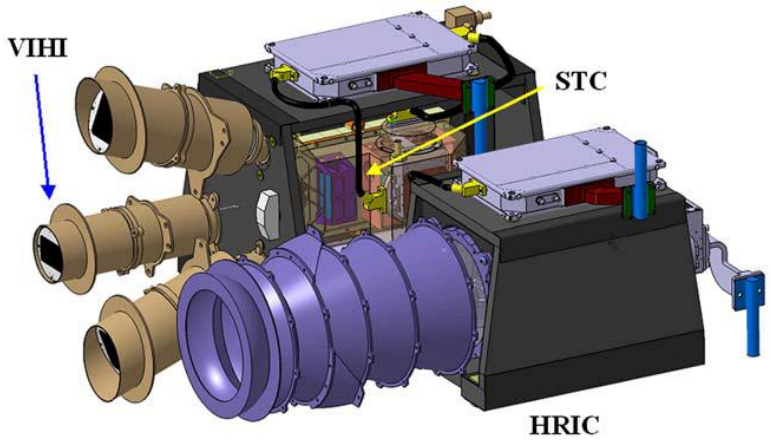

Figure 14: Graphical overview of the SIMBIO-SYS payload (Flamini e et al. 2010)

5.1.2 Observations computation

At the very beginning of the core routine, all the kernels relative to the planetary ephemerides and MPO trajectory are loaded. After the definition of the input parameters, the state vector of the probe is derived at the current epoch and following at regular time intervals as arranged in the settings of the simulation. The only issue that is important to keep into consideration is that epochs should be close enough to avoid the presence of blank spaces on the ground observations.

In order to establish what part of the surface beneath is seen and to associate it to a reference in terms of latitude and longitude coordinates, the surface of Mercury has been discretized according to a matrix as if it were projected on a Mercatore map, see Figure 11. Therefore, a cell grid is defined according to a finesse that can be set in the input parameters. For all the simulations that will be shown in the present work a matrix 770×1540 has been selected, where the center of each cell represents the node to which all the information relative to the passage are referenced. The dimensioning was made searching for the minimum values in order to simplify the computation as much as possible, that still were assuring to capture at least one node in the ground area. In fact, this may not be possible if the grid is too sparse. The calculus is easily done considering the side of the minimal ground area captured by HRIC and knowing the value of Mercury's radius.

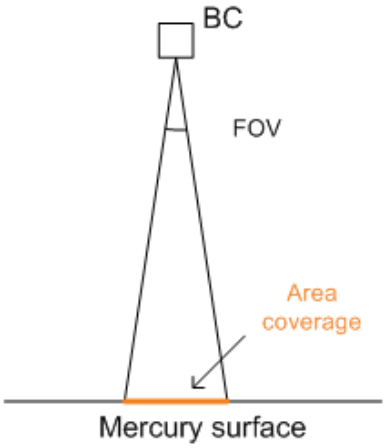

Figure 15: Illustration of the ground area covered by the on-board camera

The maximum and minimum size of the surface area covered by the camera are computed for the extremes of the orbit since it is important to have an idea of this data both at pericenter and apocenter. Since the altitude h in this two points is known, as well as the field of view (FOV) of HRIC, equal to 1.47°, one can compute the side of the area coverage l, assuming to observe a flat surface and neglecting the surface curvature, Figure 15:

$$l = 2h \tan\frac{FOV}{2} \tag{5.1}$$

The minimum ground area is of course at pericenter with a side of 10 km, as summarized in Table 6.

	Ground area size [km]
Pericenter	~ 10
Apocenter	~ 39

Table 6: Ground area size at pericenter and apocenter

The computation of the minimum number of divisions for the grid is then performed considering the maximum circumference in terms of parallels, which is obviously coinciding with the Equator. In fact, the more one moves towards higher latitudes the more the cell is representative for a smaller region on the surface of Mercury. The result has been conservatively increased and a separation in 1540 cells in the direction of the meridians has been chosen. Consequently, half of this value is used to reference the parallels.

Each cell is represented by a node, the central point of the considered sub-region, to which all the information relative to the passages are referred. The procedure employed for the computation of the ground tracks and the generation of a database is following explained:

- The state vector of the spacecraft is extracted from the kernels
- From the knowledge of the S/C position the subprobe coordinates are derived and the ground area seen by the camera is identified
- The nodes of the grid captured by the camera are identified
- The illumination conditions of the subprobe point are computed in terms of azimuth and elevation angles as well as the Mercury mean anomaly at the current epoch
- Solution of the Kepler equation for computing the eccentric anomaly and following Mercury's true anomaly
- Once the region captured by the camera is identified, a multidimensional matrix storing all the interesting information is updated with the data of the current ground-track that are added to the ones of the previous passages; the information relative to the passage are associated to the node, i.e. to a latitudinal/longitudinal reference on the surface
- A database containing all these data is generated in order to make the simulations data available for successive post-processing and analyses

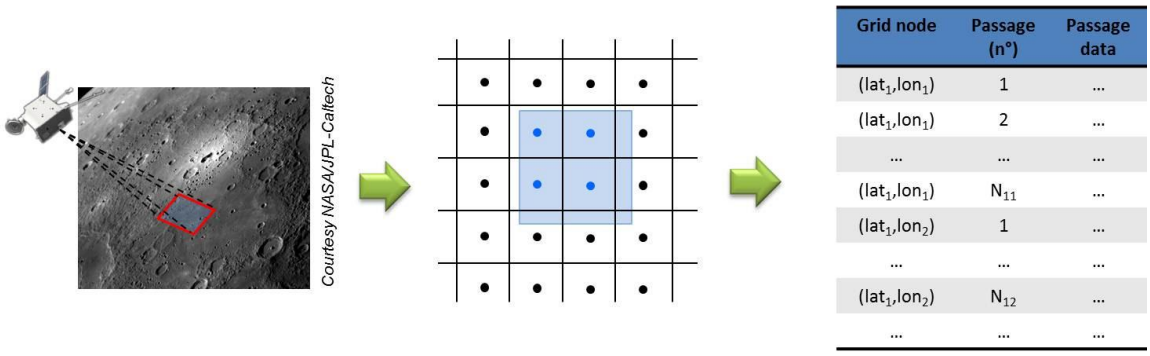

Figure 16: Illustration of the procedure for the computation of the database of the observations in the core S/W

The figure summarizes the principal steps performed inside the core routine of the observations software. First, starting from the beginning of the mission the S/C state vector is computed at each selected time interval and the ground area seen by the camera is computed. Successively, the correspondent nodes in the grid are identified and the data relative to the passage are update in the matrix collecting the information for each of them

The typical output contained in each cell of the matrix representing the database is shown in Table 7.

N° passages [#]	Epoch [ET]	Altitude [km]	Azimuth [rad]	Elevation [rad]	Mercury Mean Anomaly [rad]	Mercury True Anomaly [rad]
1	. . .	. . .	. . .	. . .	. . .	. . .
. . .	. . .	. . .	. . .	. . .	. . .	. . .
N	. . .	. . .	. . .	. . .	. . .	. . .

Table 7: Data of the passages pertaining to a single cell of the grid

In the first column the number of passage on that node to which all the data recorded on the row are referred is reported. Successively, the current epoch of the observation is displayed, unambiguously identifying the position of the S/C when employing the same kernels for the simulation.

Hence, azimuth and elevation of the Sun on the surface area interested by the current observation are listed. The determination of the illumination conditions including both angles is fundamental to provide the data necessary for the generation of the synthetic images and for driving the pattern matching procedure. Nevertheless, the first objective is to state whether the feature is illuminated or not.

Starting from the value of the altitude one can derive the variation of the scale that will be necessary to generate the synthetic images, as well as derive information on the resolution and compute the errors affecting the observations.

Instead, Mercury mean anomaly is needed to provide a preliminary estimation of the libration. Although its amplitude is not perfectly known, at this stage only an approximate level of precision is required. The libration behavior in time is modeled as a sinusoidal wave starting at the Mercury pericenter (that is the minimum axis of inertia is aligned with the Sun-Mercury direction at this point of the orbit), according to the following relationship:

$$\theta_{libration} = \lambda \sin MA \tag{5.2}$$

Where $\theta_{libration}$ is the libration angle, λ the maximum amplitude of the libration at the Equator and MA the Mercury mean anomaly. By computing the libration in this way it is possible to have an idea of the differential value appreciable between the comparison of two images taken at different epochs.

In the ground track coverage relative to one nominal mission year is presented with no filter applied apart for the obvious requirement that the surface must be illuminated. For a better understanding, high latitudes observations were cut since characterized by a number of observations so high that it was impossible to appreciate the color scale. As expected, a significant

increase of the observations exists towards higher latitudes. The two vertical stripes distinguished by an higher number of observations can be explained with the fact that the simulation was run for a duration of one terrestrial year, that is 365 days, a duration exceeding of some days twice the period of one Mercury day. This means that Mercury has already performed 6 complete rotations around its axis and 4 revolutions around the Sun, which would end with a uniform coverage of the planet surface. The days in advance determine that a portion of the surface is more observed than the others.

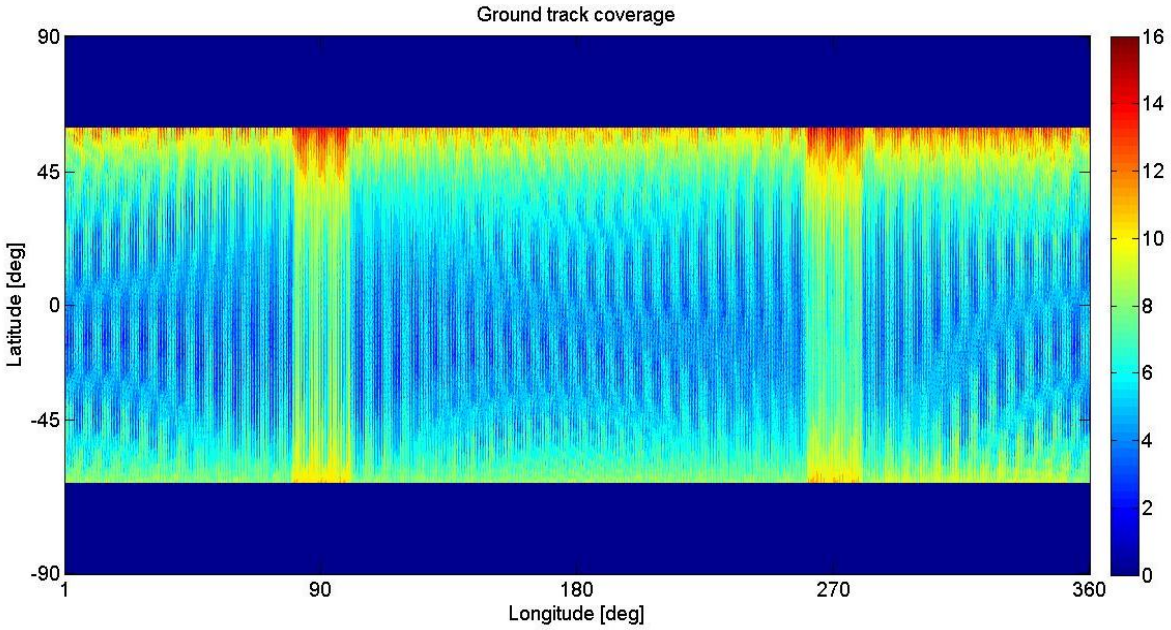

Figure 17: Ground track coverage during the nominal mission duration equal to one terrestrial year

Chapter 6

Selection of image pairs

The previous chapter illustrated the implementation of a software for the generation of a database containing the information relative to the ground tracks. The graphical output is a map of the observations that shows the number of single images that can be captured on a specific area. In order to proceed in the simulation of the overall experiment, the couples of images that can be obtained for each area of the surface need to be computed and this is the aim of the selection module.

6.1 Image pairs computation

As anticipated, the results obtained from the observations software alone are not sufficient to provide an understanding of the data available for the rotation experiment since they only refer to the single ground track and not to the crossover.

Hence, another software was implemented aimed at the investigation of the possible combinations of image pairs available for the rotation experiment. The post-processing routine takes in input the database built by the previous software and for each cell grid representing Mercury's surface analyzes the observations and examines the image pairs generated by their combinations. The couples are then filtered imposing the desired constraints in order to restrict the domain of the possible solutions according to the ones that fit the pattern matching algorithms or the physical parameter of observing a minimum libration displacement.

This last condition, ad example, is something that will be determined more precisely during a simulation campaign testing the estimation software and finally represents the output of the optimization process. At the moment in fact there are no certainties about the necessity of obtaining acquisitions in a precise area nor regarding the illumination conditions which are absolutely recommended. It could be that one particular image pair presents a very high signal in terms of libration angle but the illumination conditions makes impossible a correlation between the images or lead to a very bad accuracies.

The objectives of this module can be summarized as in the following list:

- Sensitivity analysis: influence of the observational parameters on the numbers and location of usable image-pairs

- Providing drivers for the pattern matching process

- Starting point of the iterative procedure aimed at identifying the science operations scenarios for optimizing the estimation of rotational parameters

6.1.1 Constraints

One of the objectives addressed by the work on the images elaboration and implementation of ad-hoc pattern matching strategies is exactly the study of the environmental conditions at which the experiment can be carried out. Until now, other studies performed on the rotation experiment took as a reference the work by Jorda and Thomas (Jorda e Thomas 2000). The result of their study was that accuracies of a certain level were obtainable under determined conditions of illumination thus resulting in discarding a considerable part of the available data due to unfavorable situations.

The study was performed making assumptions on the morphology of the surface and the characteristics of the visible features. In particular they concentrated on the structures of craters and the so-called albedo features, spots showing a high contrast in brightness or darkness with adjacent areas. Albedo is connected to the reflectivity of the electromagnetic radiation and its magnitude depends on the phase angle, i.e. the incidence of the Sun on the surface, and can be used to infer the presence of regolith on the terrain. Albedo can be differentiated into two types: geometric and bond. The first one is the ratio of the actual brightness at a phase angle equal to zero and an idealized flat, Lambertian disk with the same cross-section. Bond albedo is the fraction of power in the total electromagnetic radiation incident on the surface with is scattered back and takes into account all the phase angles.

In their study, Jorda and Thomas developed a software for the generation of synthetic images and assumed a plain terrain with uniform Hapke parameter, excluding the albedo features, and containing two types of craters or albedo spots. Hence, simulations were run employing the images generated and testing three different pattern matching techniques respectively based on a chi-square difference, the absolute deviation and the correlation function between the images.

The test campaign led to elect the chi-square difference method as the one restituting the best results. As far areas characterized by the presence of craters are concerned, accuracies better than one pixel are obtainable if images obtained at angles lower than 10 degrees and with shadows are discarded. Moreover, the image pairs selected must present differences in the phase angles lower than 35 degrees. These constraints permits to obtain average accuracies better than 0.5 degrees, with the worst cases touching the 0.7-0.8 pixels.

The other simulations are referred to albedo spots areas, being these features present with a certain probability in the basins and the regions populated by the rests of craters eruptions. In this

case, the conditions allowing to obtain accuracies better than one pixel are that the solar incidence is not close to the Zenith, precisely of an angle of 5 degrees, and that the Sun elevation above the horizon exceeds the 35 degrees, as shown in Figure 18. Respecting these constraints could even lead to an average accuracy better than 0.5 pixels.

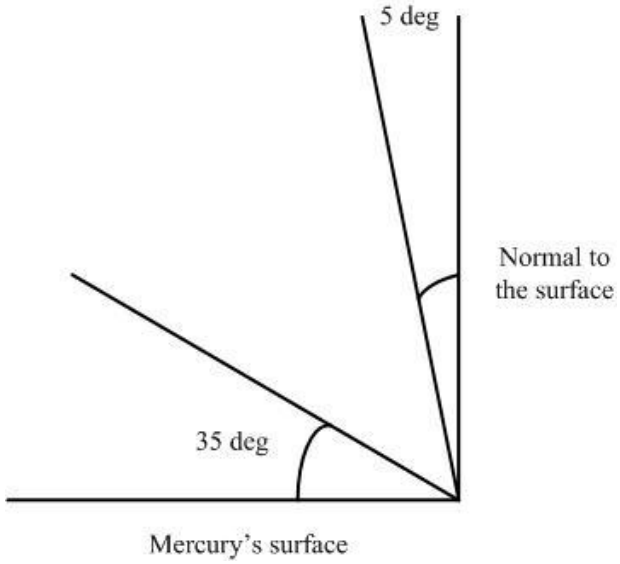

Figure 18: Constraints on the Sun elevation angle on the surface of Mercury

Other limitations that could be considered were also thresholds imposed by the maximum altitudes. Ad example, in the work by Pfyffer (Pfyffer 2010) some simulations were run to show the influence of limiting the height to 1000 km. Obviously, the number of observations and image couples at disposal is lower. An advantage of dealing with these constraints is that pictures at higher resolutions are available since the approaching of the S/C to the apocenter is inevitably resulting in a decrease of this parameter. Consequently the quality of the images is higher and pattern matching phase is further facilitated by the fact that the changes of scales in a pair will certainly be more contained.

Thanks to ad-hoc built algorithms the team working on the elaboration of the images is confident that most of these constraints can be relaxed, thus allowing a significant increment in the number of useful image pairs. This could have important consequences on the mission output since permits to keep acquisitions that could give a good contribution to the overall accuracy of the estimation process.

Despite this reasoning and still taking into account that the possibility of choosing among all the possible observations is precious, being the optimal science planning so undetermined, is not univocally certain that the observations taken under some conditions such as the ones on the altitude or illumination. This is clear looking one of the results obtained by Pfyffer et al. (Pfyffer, Van Hoolst e Dehant, Librations and obliquity of Mercury from the BepiColombo radio science and camera experiments 2011) in the simulation where constraints on the maximum altitude were introduced: this limit was actually detrimental for the determination of obliquity and planetary

induced librations by Jupiter and Venus but beneficial for the estimation of Mercury's libration amplitude.

Before giving an explanation to this output, it must be underlined that the parameters used to select the image pairs are that a certain number of couples is randomly chosen among the database of the possible ones. When cutting the images taken at the higher altitudes it is obvious that also some of the observations captured in this conditions are discarded. This determines that the signals employed for the estimation of the librations are stronger thanks to the higher presence of observations in the equatorial regions and the fact that periherm is close to the equator. On the contrary, adding the solutions taken at higher altitudes introduces a degradation caused by lower resolution images.

The determination of the obliquity showed the opposite behavior with respect to the limitation in the altitude and the explanation is clear when analyzing the dynamics of the BepiColombo trajectory around Mercury and the orbit of the last one around the Sun. The beta angle of MPO's trajectory is equal to 0° and Mercury presents a 3:2 spin-orbit resonance thus determining that out of three observations taken on the dayside two are relative to low altitude images captured at periherm when Mercury is located at the aphelion while the third corresponds to high altitude observations at apoherm around Mercury perihelion. The two observations taken at low altitude are almost symmetrical about perihelion and present no differential information on the obliquity. The one which is really providing the fundamental signal is the image taken at the higher altitude since it offers a difference in the viewing angle of the obliquity. For this reason the exclusion of the observations collected on the apoherm side is deteriorating the estimation of the obliquity.

It emerges then the importance of executing an optimization procedure of the science planning since it is not trivial to determine the conditions which are beneficial for the estimation of both the rotational parameters. It is necessary to encounter a trade-off between the two options.

Should the outcome of the optimization algorithm state that image pairs collected at high altitudes are crucially important for the success of the experiment or guarantee very good accuracies in case the problem of correlating image pairs characterized by too elevated changes of scales the possibility exist to remedy by means of advanced observational techniques. This is one of the innovation propose by the CVG team working on the elaboration of the images, who suggested the introduction of a strategy such as the super-resolution, see paragraph 9.5. This approach consists in collecting a sequence of images of the same portion of the surface at high frequency. The over sampling of the chosen area permits, after an adequate post-processing, to increase the resolution of the image up to four times. This means that the same resolution of 5 m/pixel obtainable at periherm are also possible for the apoherm observations. The only problem presented by the employment of this technique is that it requires a considerable increase in the dedicated data volume since more images are needed and limitations in the maximum number of images at disposal for the rotation experiment exists. Again, this is something that will be clear only after an extensive simulation campaign and the finalization of the mission capabilities.

6.1.2 Software architecture

As for the observations software, this program is composed by two main routines: the first one is used to define all the input and output folders as well as the global and the simulation parameters to be used while the other one represents the core program where all the principal computations are made and the subroutines called.

Basically, the software is outlined as follows:

- The input parameters and simulation settings are loaded
- Definition of the constraints on the singular observations
- Definition of the constraints on the image pairs
- Retrieval of the database of image pairs relative to the cell grid under examination (this step is repeated for each node of the grid representing Mercury's surface)
- Analysis of each possible combination in couples among the observations regarding the cell and check of the constraints imposed
- Generation of a database of image pairs

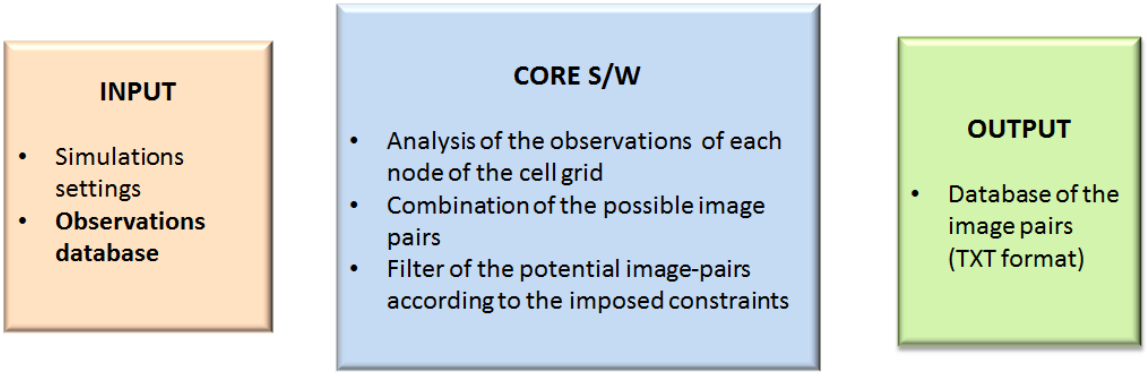

Figure 19: Architecture of the core routine of the selection software

In particular, a clarification is needed regarding the meaning of imposing constraints on the singular observations and the image pairs. This is referred to the fact that the observations are first filtered according to their compliance with some requirements, that could be either a simulation parameter (time for example) or a physical constraints (such as illumination conditions) and after this first selection image pairs are formed. The couples obtained are then further filtered applying conditions on the differential values of some data relevant for the selection of the image pair. For

example a condition could be that the difference in altitude should be limited in order to avoid high changes of scale.

At the moment, the constraints that have been set in the software are highlighted in Table 8. Basically, the ones that are normally used to derive the number of the image pairs available for the experiment are the azimuth and elevation angles determining the illumination conditions, the altitude, and the estimated visible libration.

Constraint		**Singular observation**				**Image pair**	
Time		ET_{in}	Initial Epoch	ET_{fin}	Final Epoch		
Altitude		a_{min}	Minimum	a_{max}	Maximum	Δa	Differential
Mercury True Anomaly	Exclusion zone 1	θ_{min}	Minimum	θ_{max}	Maximum		
	Exclusion zone 2	θ_{min}	Minimum	θ_{max}	Maximum		
Azimuth		Az_{min}	Minimum	Az_{max}	Maximum	ΔAz	Differential
Elevation		El_{min}	Minimum	El_{max}	Maximum	Δel	Differential
Libration						Δlib	Differential

Table 8: Constraints that can be imposed in the selection procedure

Among the setting options offered by the software is also the possibility of introducing limits on the true anomaly exclusion zones. The presence of such a type of constraint is due to the current issues the BepiColombo mission is experiencing in guaranteeing a full coverage of the science operations all over its duration. During the manufacturing of the spacecraft problems arose concerning thermal resistance of the solar panels. In order to prevent them from undergoing too stressing thermal loads, they must be rotated with respect to their configuration guaranteeing the maximum production of power. This results in a limitation of the science operations in the periods where this situation occur, that is close to perihelion and to aphelion.

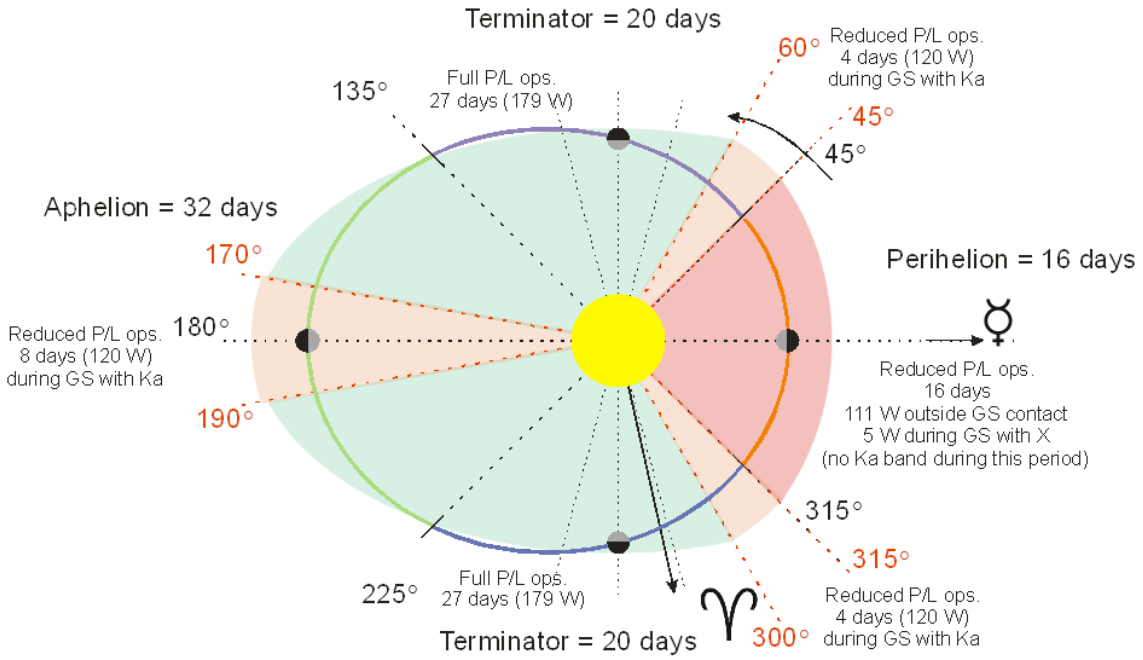

Figure 20: BepiColombo power limitations in Mercury's orbit around the Sun (Hoofs, Middleton e McAuliffe 2010)

Although the presence of reduced power operations seems quite serious at the moment, it was decided not to include these constraints in the simulations. In fact, it is not yet established how the radio science experiment will be affected by this scenario and the possibility exist that if some observations are needed for the rotation experiment in these phases, they might be granted.

Hence, the first thing which is important to understand is demonstrating the real necessity for the success of the experiment of having a certain number of observations belonging to this time period. This point will be cleared after the conclusion of the campaign test on the optimization software.

6.2 Simulation results

The first simulation was run without imposing any constraint in order to have an idea of the global picture regarding the number of image pairs potentially available. The result is displayed in Figure 21. As obvious, the number of couples is much higher than the number of the singular observations since they depend on their combination.

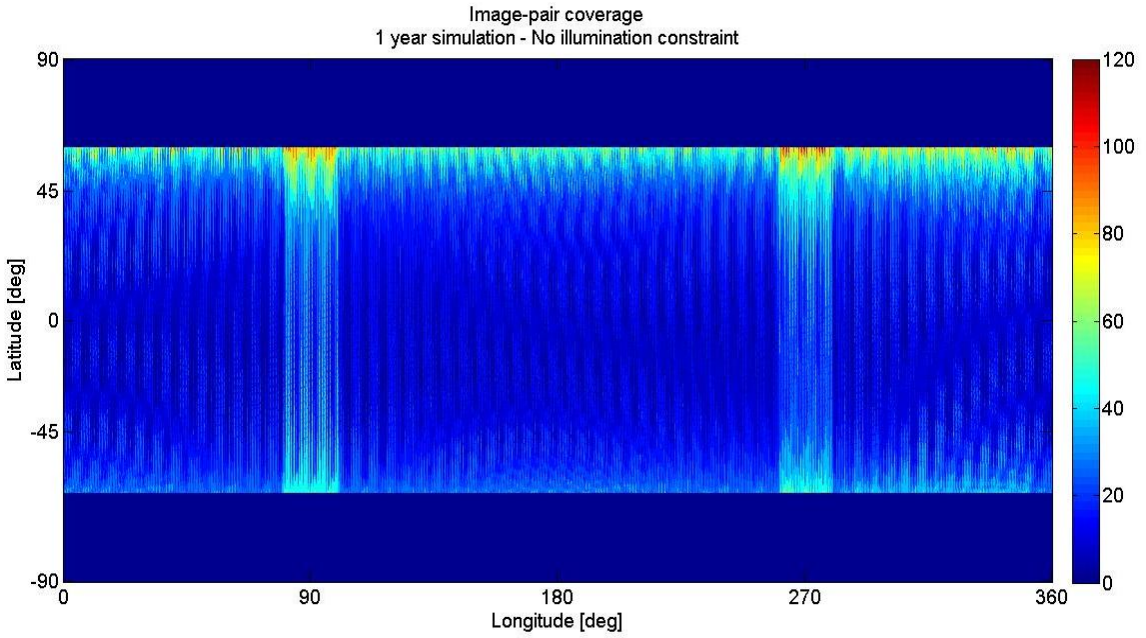

Figure 21: Image pairs coverage for one nominal mission year

Successively, the results are filtered according to the desired constraints which are separately specified in a setup routine. As already mentioned in the previous sections, until now all the simulation hypothesis were based on the work by Jorda and Thomas who excluded a considerable part of the available data due to unfavorable condition for the pattern matching. Thanks to ad-hoc built algorithms the MORE team is confident that most of these constraints can be relaxed, thus allowing a significant increment in the number of useful image pairs.

Since different pattern matching strategies apply according to the different conditions at which images will be collected, simulations were performed in order to drive this process and determine the most frequent scenarios. In fact, scale invariant "gradient based" features (SIFT,SURF, …) are best suited for limited changes in sun elevations and very limited changes in azimuth angles between the image pairs, but are able to handle even pictures taken at high and low phase angles. They offer a very good accuracy up to the order of 10^{-2} pixels and as sparse descriptors they do not depend on the type of geometric features detected in the images, such as craters plains and ridges. The last ones are instead used when moderate changes in illumination in the image pairs exist. A preprocessing of the image is required to attenuate these variations (through phase congruency, for example) and to identify crater rims and centers, or other morphological features. In order to deal with situations of abrupt changes in illumination, transformed feature space (Size Functions, …) and combined matching and Shape From Shading (M&SFS) are the preferred candidates.

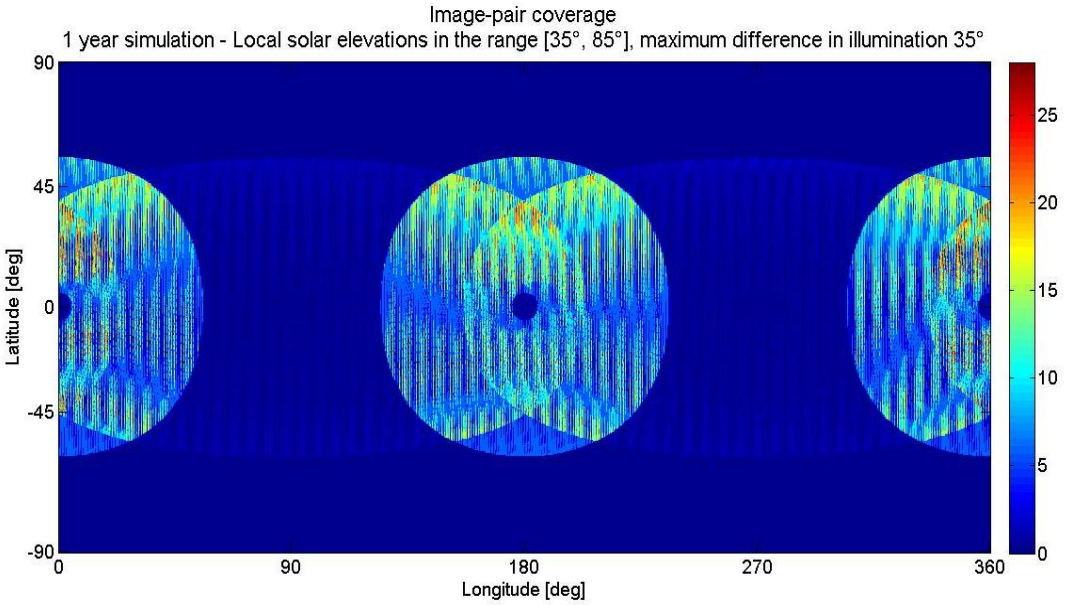

In order to show the possible cases in which the first type of algorithms described can be employed, a simulation was run imposing as constraints changes in azimuth and elevations lower than 10° and 35° respectively, and excluding the extreme conditions for the phase angles, limiting its variation in the range of 5° and 85° (Figure 22). Although observations are more frequent in certain areas, it is possible to notice a good coverage over the majority of Mercury's surface. Obviously, a significant increase occurs starting at 60° of latitude.

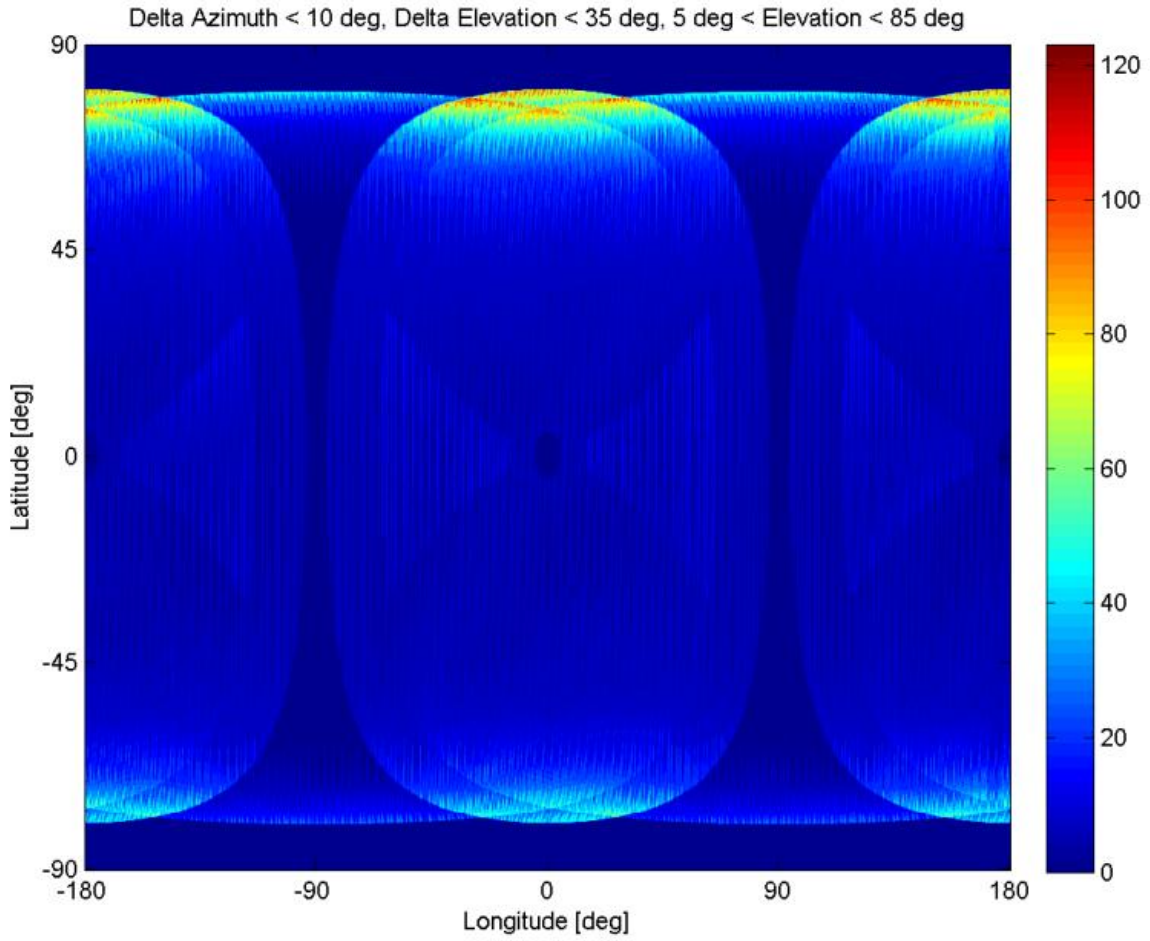

Figure 22: Image pairs map obtained imposing the following constraints:Δazimuth<10°, Δelevation<35°, 5° < elevation < 85°

Since depending on the algorithms also the robustness to changes of scales could affect the accuracy of the pattern matching, a further constraint limiting variations in altitude to 700 km was imposed leading to very similar results, as shown in Figure 23. It is also interesting to point out that if a constraint on a minimum value of libration is added no matching results are obtained. This is consistent when thinking at the dynamics of the problem for which no libration is visible at the same mean anomalies, i.e. the same illumination conditions.

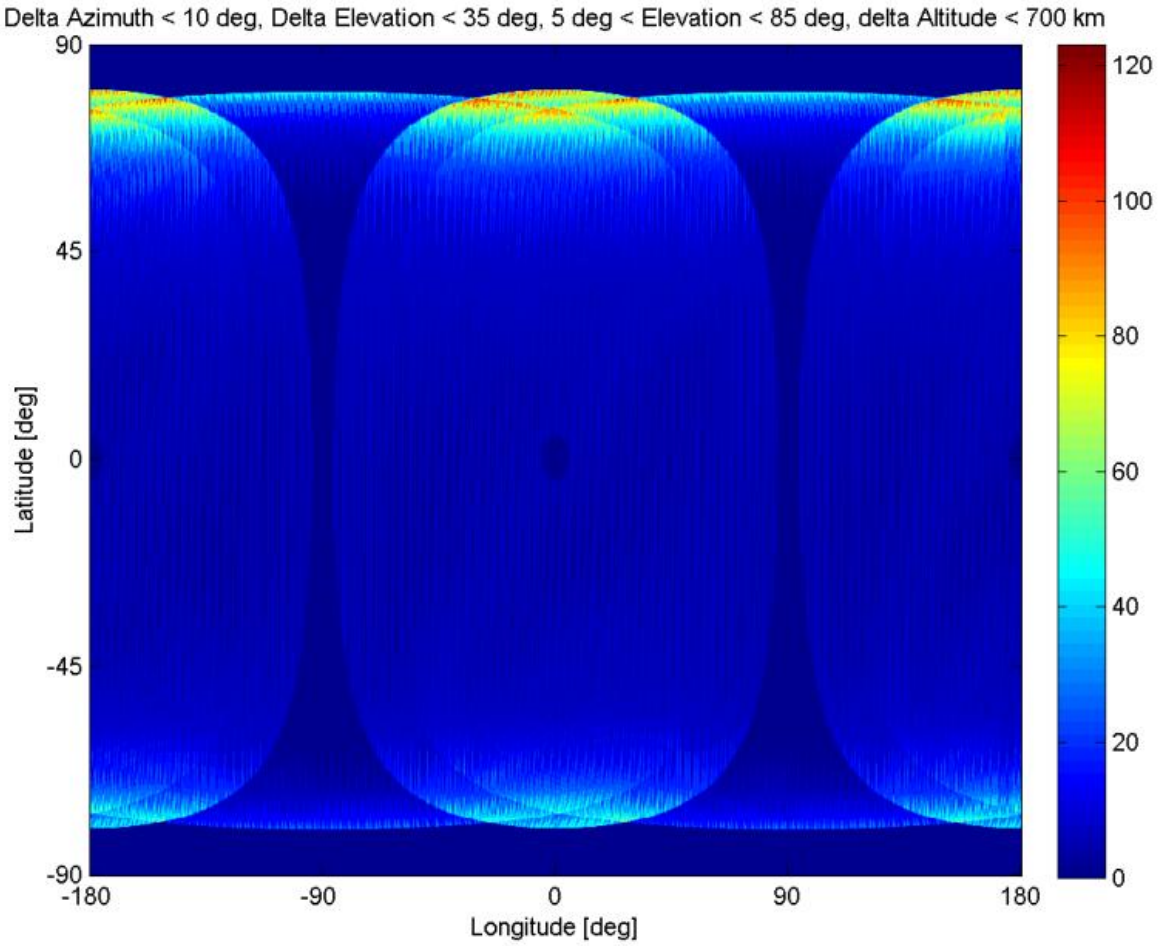

Figure 23: Image pairs map obtained imposing the following constraints: Δazimuth<10°, Δelevation<35°, 5° < elevation < 85°, Δaltitude<700 km

From the point of view of the estimation of the librations, it could be also interesting to see were the highest deviations can be appreciated. In Figure 24 results relative to libration amplitudes higher than 500 m are displayed (librations can be in the range [0-800] m). As expected, image pairs are concentrated at latitudes lower than 45°, with a maximum between 35° and 45° since these regions are the ones characterized by the highest number of potentially useful image pairs that could satisfy the imposed constraints.

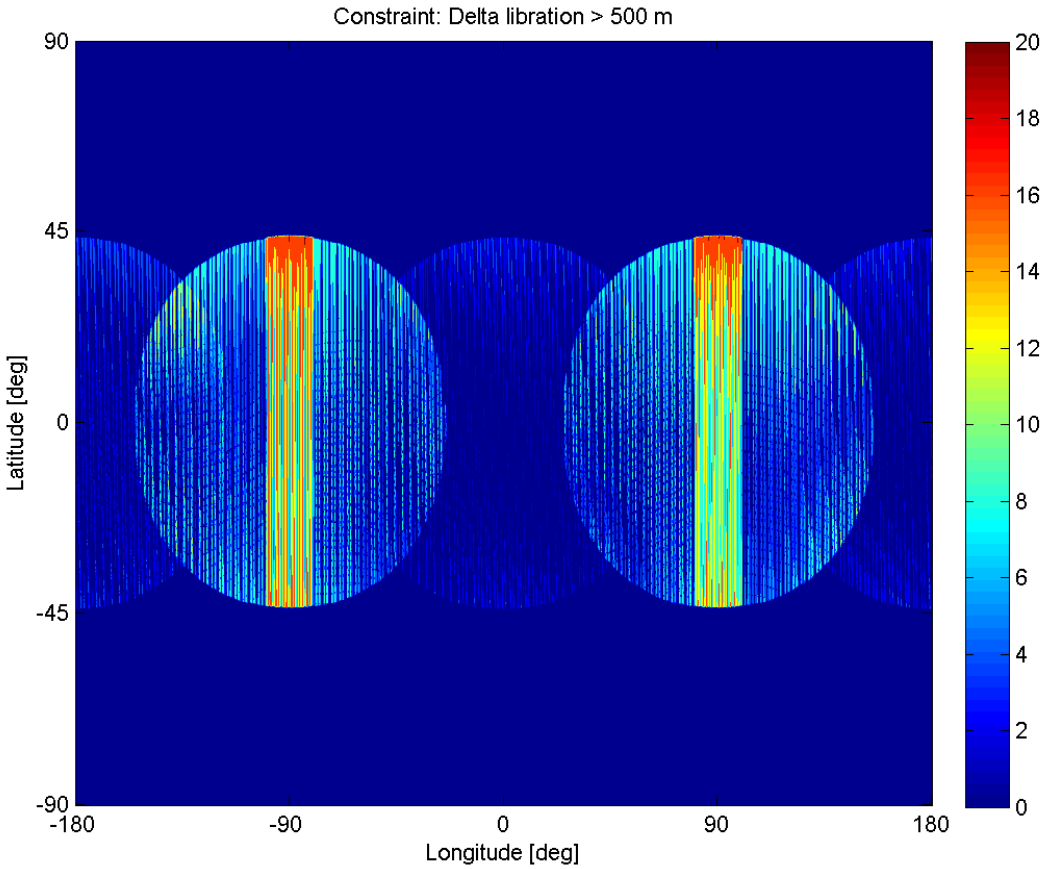

Figure 24: Image pairs obtained imposing a constraint of a minimum observed libration of 500 m

Among the proposed observational strategies, the super-resolution technique was deemed particularly attractive since able to enhance the image resolution up to four times. Consequently, a significant number of observations initially discarded due to poor quality (or an inferior quality with respect to the one obtained when flying closer to periherm) could be saved. Moreover, since it is likely that in the correlation phase images taken at very different altitudes, and hence at very different resolutions, must be compared, this technique could grant the possibility of improving the resolution of the poorest image thus easing or even making successful the pattern matching process. In Figure 25 simulations relative to global results filtered depending on a maximum value of the altitude, respectively 700 km, 900 km and 1200 km are shown, zoomed on the right part for better appreciating the color scale. The aim of this analysis is to highlight the impact of constraining the altitude in the overall amount of obtainable image pairs that could effectively be used in the estimation process. In fact, if only high resolution images are taken into consideration the number of couples significantly decrease so demonstrating the positive contribution that acquiring images in super-resolution mode would introduce in the experiment.

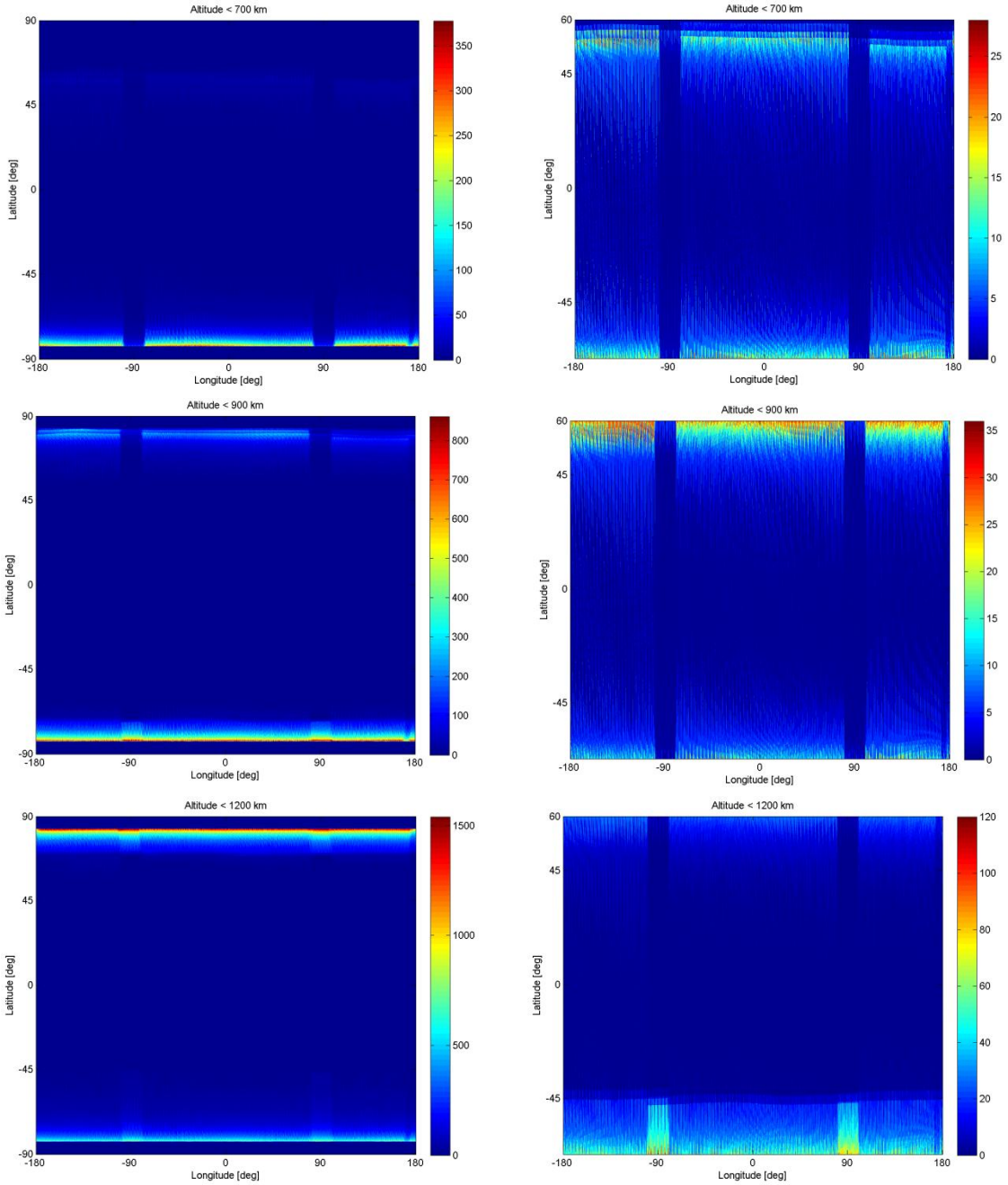

Figure 25: Comparison of image pairs obtained imposing a constraint on the altitude.

Three cases are shown respectively referred to altitudes lower than 700 km, 900 km and 1200 km (maximum apoherm altitude equal to 1500 km). On the left side the complete coverage over the entire surface is shown, while on the right side a zoom is performed in order to better appreciate the color scale

Chapter 7

Optimization module

This chapter deals with the implementation of the optimization module which is probably the most critical part in the end-to-end software simulating the rotation experiment. The genetic algorithm selected for dealing with this procedure is presented and the preliminary simulations are shown.

7.1 Genetic algorithms

A genetic algorithm is a search heuristic technique which derives its behavior from a metaphor of the processes of evolution in nature. Heuristic means that the method is based on the experience for problem solving, i.e. the solution would rather said to be estimated than being calculated. Furthermore, genetic algorithms are stochastic (probabilistic) methods, not deterministic. This is one of the main difference between GA and the other heuristic algorithms and the other significant distinguishing element is that it works on a population of possible solutions while other heuristic method use a single solution in the iterations.

GAs are particularly adapt to those problems untreatable with standard techniques such as gradient ascent or additive approximations. Typically, it is difficult to formulate an exact and accurate mathematical translation for the problem and it may contain noisy or irregular data, or require computational times which are too high or are simply impossible to be solved employing traditional computational methods.

Genetic algorithms start the optimization process from a set of solutions, a *population* of strings, each of them called *chromosome* or genotype of the genome. A chromosome consists in a string of symbols, called *genes*, traditionally represented as binary numbers, even if other encoding options exist. These chromosomes encode candidate solutions, also referred as individuals, creatures or phenotypes, aimed at an optimization process where they evolve toward better solutions.

The evolution usually departs from a population of randomly generated individuals and through successive iterations evolves in *generations*. In each generation, each individual is evaluated by means of a *fitness* function ad-hoc defined for the specific problem to be solved. In order to form the next generation, multiple individuals referred as *parents* are stochastically

selected from the current population (based on the fitness function previously computed) and used to create new chromosomes, traditionally called *offsprings*. Solutions which are not selected for the *reproduction* are discarded, so chromosomes characterized by and higher fitness function are more likely to be the candidate for the generation of the offsprings. This passage takes place via two processes: the combination of two parents chromosomes belonging to the current generation by means of a *crossover*, and the random modification of the chromosomes through a *mutation*. The new population is then employed for the next iteration of the algorithm.

Usually, the algorithm terminates when a stopping condition is reached:

- maximum number of iterations is reached
- convergence to best chromosomes representing the optimal solution of the problem
- computational time limit
- a plateau is reached by the best ranking solution so that successive iterations are not bringing any improvements

Genetic algorithms work on two types of spaces alternatively at each iteration:

1. coding space (genotype space)
   Crossover and mutation are genetic operators working on genotype space, and imitate the inheritance process of the genes of each chromosomes to create a new population.

2. solution space (phenotype space)
   Evolution and selection work on phenotype space. The first one imitates the evolution process of Darwin for the creation of a new population of better individuals in the sense defined by the fitness function. The selection process represents the connection between chromosomes and the performance of the decoded solutions

Summarizing, the procedure used for the genetic algorithm is the following:

(a) Choose the initial population of individuals
(b) Evaluate the fitness of each individual in that population
(c) Repeat on this generation until termination (time limit, sufficient fitness achieved, etc.):
   - Select the best-fit individuals for reproduction
   - Breed new individuals through crossover and mutation operations to give birth to offspring
   - Evaluate the individual fitness of new individuals
   - Replace least-fit population with new individuals

The process is also depicted in Figure 26.

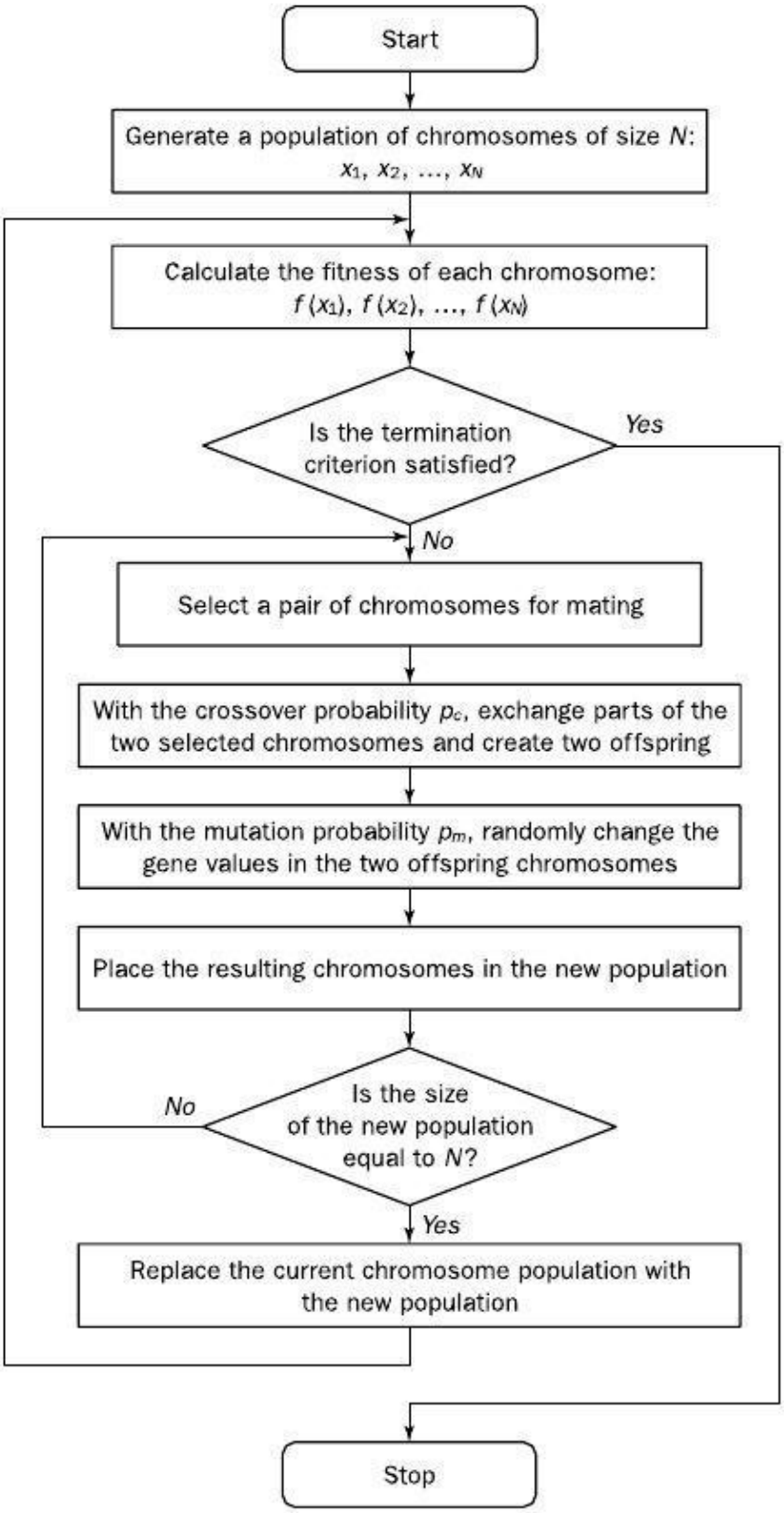

Figure 26: Genetic algorithm flowchart

7.1.1 Performances and implementation recommendations

A critical point for the success of GAs is represented by the mapping from genotype space to phenotype space, step which has a considerable influence on the performance of genetic algorithms.

Genetic algorithms main property is the capability of providing a directed random search in complex landscapes. Two important issues must be taken into account when dealing with search strategies: exploration (investigate new and unknown areas in search space) and exploitation (make use of knowledge of solutions previously found in search space to help in find better solutions). This can be done by making genetic operators perform essentially a blind search and hoping that selection operators direct the genetic search toward the desirable area of solution space.

One general principle valid during the implementation of genetic algorithms for a particular real world problem is to introduce a good balance between exploration and exploitation of the search space. To achieve this, it is wisely recommended to carefully examine all the operators and parameters of the genetic algorithms.

7.1.2 Application of GAs to the rotation experiment optimization problem

The problem to be solved, consisting in the optimization of the science observation plan of the BepiColombo rotation experiment, is highly non-linear, as well as difficult to be described and defined under a deterministic point of view. For this reason, the choice of the algorithm to be used for the optimization fell onto the genetic algorithms, since they seemed the most tailored to the problem.

The definition of the optimal science observations plan is quite complex and still some details of the mission are under development, so the very definitive solution is far from being frozen in the immediate future. Some aspects regard the eventuality of exclusion zones during the missions where scientific activities could be suspended due to thermal issues, see section 6.1.1.

In the specific case the aim of the genetic algorithm is finding the set of image pairs which allows to obtain the best estimation of the rotational parameters of Mercury. The problem is not trivial because of the vast domain of the solutions: the surface of Mercury where the observations can be picked up is divided into a 770x1540 cell grid. In turn, each cell contains a list in form of a database of the possible image pairs that can be collected under the constraints imposed by the selection module. This significantly expands the domain from 770x1540 sets of solutions to one equal to the total number of image pairs.

Since the one presented in this work is the first compilation of the genetic algorithm and from the moment that an adequate debugging campaign is needed to explore every single aspect of the algorithm implementation, a simplification was introduced consisting in the fact that for each cell only the first image pair contained in the database is selected. It is indeed true that this condition is detrimental for the finding of a global optimum, but this step is fundamental for understanding step by step the functioning of the procedure. Furthermore, an adequate strategy for

the employment of all the image pairs relative to one node of the matrix is necessary. The space domain was in fact encoded starting from the latitude/longitude reference so a way to handle a set of different image pairs referenced to the same geographical point must be found.

7.2 Encoding

One of the fundamental aspects when dealing with GAs is the encoding of the search space domain, which means codifying one solution into a chromosome. This step is crucial since it is strictly connected to the problem. There exist different type of encoding even if traditionally the method more simple and flexible is the binary encoding. Anyway, several encoding methods have been explored, not in a string form but employing integer and real number.

Following the different type of encoding are presented (Obitko 1998).

7.2.1 Binary encoding

Binary encoding is the most common type, mainly because of tradition since the first analyses about GA used this type of encoding. In binary encoding chromosomes are translated as string composed by sequences 0's or 1's bits. As already pointed out in section 7.1, each chromosome is an array of genes representing a solution (Chakraborty 2010).

Hence, genes appear as illustrated in Table 9, while an example of chromosome is shown in Table 10.

#	Genes (binary encoding)
1	1101
2	1000
3	1011
. . .	
n	1110

Table 9: Example of genes representation

	gene 1	gene 2	gene 3	gene 4
Chromosome	1101	1000	1011	1110

Table 10: Examples of chromosomes in binary encoding

Binary encoding gives many possible chromosomes even with a small number of alleles. On the other hand, this encoding is often not natural for many problems and sometimes corrections must be made after crossover and/or mutation.

7.2.2 Permutation Encoding

Permutation encoding is the strategy employed in cases of ordering problems. Every chromosome is a string of numbers, which represent a precise sequence.

Chromosome	6	5	3	2	9	4	7	1	8

Table 11: Example of chromosomes with permutation encoding

Even in this case it might be necessary to introduce some corrections after the application of the genetic operators in order to obtain chromosomes belonging to the solution domain (i.e. the sequence must be consistent).

7.2.3 Value Encoding

Direct value encoding is method used in problems where the application of the binary encoding would be unfeasible. For example in cases where real numbers are used. Chromosomes are represented by a string of some values. Values can be anything connected to problem, form numbers, real numbers or chars to some complicated objects.

Chromosome	5.6571	8.1211	7.3657	1.6584	4.3239	9.0048

Table 12: Example of chromosomes with value encoding

Value encoding is particularly tailored for some problems but presents the disadvantage that new genetic operators must be ad-hoc developed.

7.2.4 Tree Encoding

Tree encoding is used mainly in order to evolve programs or expressions, for genetic programming. In tree encoding every chromosome is a tree of some objects, such as functions or commands in programming language.

7.2.5 Encoding of the solution domain for the rotation experiment optimization

A careful review of the encoding methods explained in the previous paragraphs was made in order to identify the best strategy for translating the search space domain representing the solutions for the rotation experiment.

The space of the solutions is given by the latitude/longitude coordinates of the nodes of the cell grid representing the surface of Mercury. Such nodes must be encoded in order to render the genetic operations efficient and consistent with the problem in exam. The genes should represent a spatial position in a matrix, therefore they must contain the information relative to the row and the column identifying the node. A sequence of genes would then give a chromosome, that finally results in set of image pairs observations representing one solution of the problem. At the end it was decided that the best description for a gene was the sequence in this order of the row and column encoded in binary, as graphically explained in Figure 27.

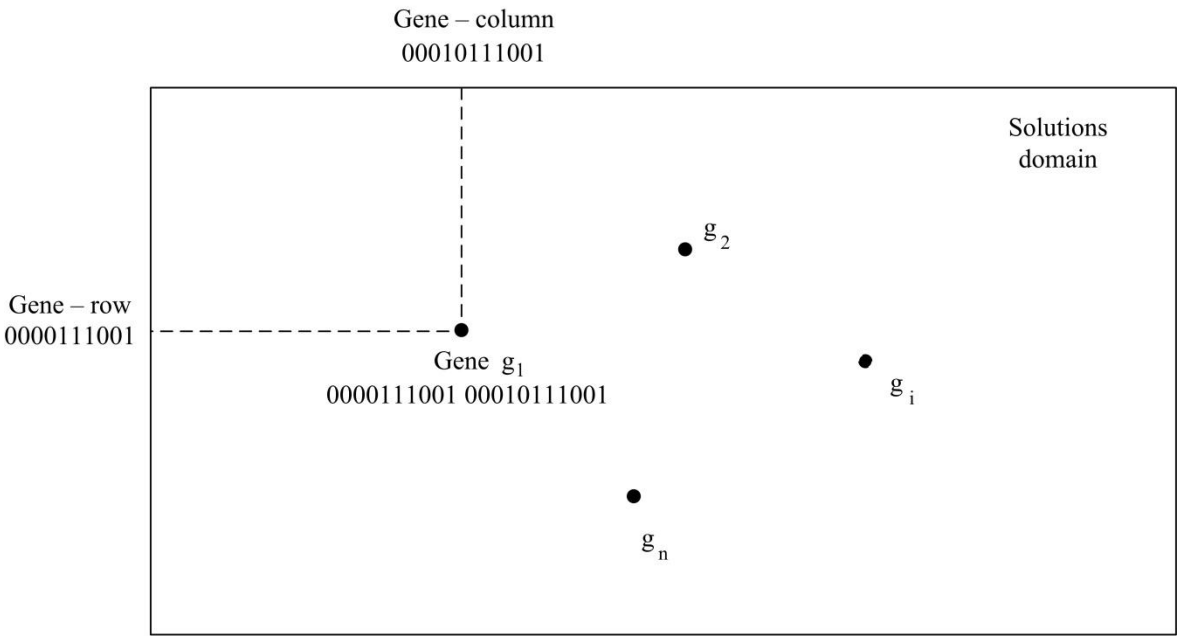

Figure 27: Graphical representation of the encoding of the space domain

One chromosome is then defined as the union of all the genes representing the observations without the order being important. In fact the genes alone represent one image pair which is following furnished as input to the estimation software.

Hence, a chromosome is represented as follows:

	g_1	g_2	g_i	g_n
Chromosome	0001101011 10110011011	0011010010 0000001011	..	1001000011 00110101100

Table 13: Chromosome representation

A subroutine recalled by the main program was implemented aimed at the encoding of the population. The routine receives in input the matrix of the solutions in decimal numerical system and operates the translation into a binary code. Since the means used to perform the successive genetic operations that creates a new population consists in the recombination of genes among the chromosomes and in randomly mutating some alleles, it seemed that a Gray encoding was more adapt to maintain a continuity in the domain.

The Gray code is also known as reflected binary code and is a binary system where two successive values differ in only one bit. The procedure for converting binary to Gray numbers is very simple and summarized in Table 14.

Binary – Gray conversion			
Binary to Gray	Binary: Gray:	110010 XOR 110010 101011	Execution of the XOR between the binary number to be codified and the same number moved one cipher to the right
Gray to Binary	Gray: Binary:	101011 XOR 11001 110010	The most significant bit of the Gray number is reported, and then the XOR is executed between the bit obtained (in the binary number) and the successive bit of the Gray code (form the left to the right)

Table 14: Binary – Gray conversion

By using this type of conversion adjacent nodes of the grid only differs by one bit and are consecutive also in the algorithm encoding as well as in the decimal representation.

Since the matrix to be encoded is a 770x1540 it is straightforward to derive the maximum dimension of the binary string representing rows and columns. In particular, the first ones must take into account that the space for a 10 bit string must be reserved, while for the second one 11 are needed. This means that as long as this grid refinement is maintained, one gene will be codified by a 21-bits string. The length of the chromosome is not univocally defined since it depends on the number of the image pairs that will be chosen for estimating the rotational parameters.

7.3 Selection

The selection procedure serves the purpose of creating a new population for the following generation. A subset of genes is extracted from the existing population Among the current population some parents chromosomes are selected for successive crossover. As well it could be decided that some of them are maintained in the following generation thanks to the goodness of their fitness function.

In this phase two different strategies could be applied:

- Regular search space
  In standard GAs the successive generation is made by chromosomes deriving from the offspring. Obviously, the possibility exists that some of the fittest individuals are lost from one generation to another. In these cases, 'replacement' methods can be applied in order to recover these chromosomes in the successive generations.

- Enlarged search space
  When using this strategy chromosomes coming from parents reproduction and offsprings have the same probability to be selected to generate the successive population. In this way, solutions characterized by an high fitness are never discarded and the probabilities of crossover and mutation can be increased (see section …) without invalidating the algorithm with the introduction of too elevated perturbations.

One of the main problems that could determine the success of GA is the choice of the more adapt strategy for selection. The methods can be divided into stochastic, deterministic and mixed. A typical stochastic method is represented by the 'roulette wheel' described in paragraph 7.3.1. Sometimes non-equality constraints among the chromosomes of the same generation are introduced so as to increase the variability of the population and avoid the stagnancy in local minima.

In the following paragraphs the more popular methods are outlined.

7.3.1 Roulette Wheel Selection

The roulette wheel is a classic stochastic method. Parents are selected according to their fitness and the more the fitness is high the more chances they have to be selected. The probability of each chromosome to be selected is represented by the amplitude of the cut on a wheel assigned to it by its fitness, see Figure 28.

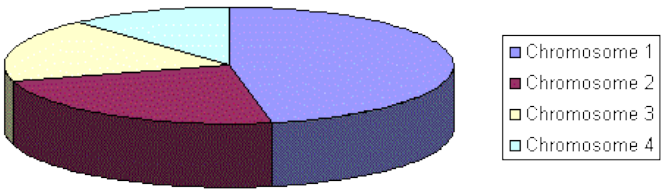

Figure 28: Roulette wheel selection (Obitko 1998)

7.3.2 Rank selection

This type of selection is used whenever the roulette wheel method is inapplicable because of the too high difference among the fitnesses. The result could lead to fact that some chromosomes are never selected while the fittest one is always chosen. By employing the rank selection chromosomes are ordered according to their fitness and depending on the position in the list they are associated to a predetermined fitness, from fitness 1 to N.

In this way, all the chromosomes have a chance to be selected but the convergence is lower due to the fact that best individuals are not standing out in the population.

7.3.3 Steady-state selection

The principle at the base of this method is that a considerable quantity of individuals automatically survive to the next generation. In each generation a few chromosomes among the ones with high fitness are selected for the crossover operation. The less fittest individuals are eliminated and substituted by the new offsprings. The remaining population survives to the next generation.

7.3.4 Elitism

The concept of elitism was introduced in order to avoid the loss of the fittest individuals due to the operations of crossover and mutation. When adopting this strategy the best chromosome or a few of the bests are directly selected to be part of the next generation. The rest of the population is treated with another method.

The advantage of elitism is the increase of the performance of the algorithm, since the best solution is never lost.

7.3.5 Selection method choice and implementation

For dealing with the optimization problem presented by the rotation experiment a selection approach which is mix of the selection methods presented in the previous paragraphs was chosen.

A certain part of the population is selected according to the principle of elitism, in order to prevent the algorithm to lose some optimal solutions. On the contrary, the individuals characterized by the worst fitnesses are discarded and substituted by new random solutions belonging to the domain so as to guarantee a constant exploration of the search space. The rest of the current population is treated with a crossover operation in order to reproduce and form the new offsprings where selection is made via the roulette wheel method. The rate at which elitism and elimination (and consequently crossover) are actuated is determined in settings of the simulation. At the moment they have both been set to a 10%.

Current population	Process operated	New population
C_1	$\xrightarrow{elitism}$ copied to successive population	C_1
C_2	$\left.\begin{matrix} C_2 & C_4 \\ C_3 & C_9 \\ C_5 & C_2 \\ C_6 & C_8 \end{matrix}\right\} \xrightarrow{crossover}$	…
C_3		…
C_4		…
C_5		…
C_6		…
C_7		…
C_8		…
C_9		…
C_{10}	discarded an substituted by a new random individual	C_{new}

Table 15: Selection method employed

A subroutine was then implemented receiving in input the matrix of the individuals in the population to be selected for successive genetic operations. The chances of an individual of being selected are proportional to its fitness. The parents that will be used for successive crossovers to generate new offsprings are derived via the following procedure simulating the roulette wheel:

- Computation of the partial sum of the fitnesses starting from the first individual to the last until the vector of the partial fitnesses is calculated:

$$F = (f_1 \quad f_2 \quad \cdots \quad f_n)$$

Chromosomes	Elements of the fitness vector
$\boldsymbol{C_1}$	$f_1 = f\|_{C_1}$
$\boldsymbol{C_2}$	$f_2 = f\|_{C_1} + f\|_{C_2}$
…	…
$\boldsymbol{C_n}$	$f_n = \sum_{k=1}^{n} f\|_{C_k}$

Table 16: Computation of fitness vector for the roulette wheel selection

- Generate random numbers in the interval $0 - f_n$
- Associate the random numbers to their position in the elements of the fitness vector so as to derive the correspondent chromosome

- As chromosomes are selected they are disposed in a matrix in couples of parents, ready for successive reproduction

7.4 Crossover

The crossover is the principal genetic operator and consists in combining two chromosomes selected as parents which mates and generate the offsprings. The underlying idea is that the new offsprings present a fitness characteristic which is better than the one of the parents. Crossover happens according to a probability that is a priori fixed before the starting of the simulation. The probability represents the ratio between the number of chromosomes (even) subjected to the crossover at each iteration and the entire population. A large crossover rate permits to explore a wide zone of the solution space and reduces the possibility of incurring into a false optimal solution. On the other side, the greater number of solutions to be analyzed induces an increase in the computational time.

In the following paragraphs some of the typical operators are presented.

7.4.1 One-point crossover

The one-point crossover is the simplest way of performing this operation. A random number is defined individuating the cutting point in the two parents chromosomes. Hence, the first offspring is generated by copying every bit before this point (in case of a binary encoding) from the first parent and every bit after the point from the second parent. Analogously for the second offspring. The process better clarified in Table 17.

Parent 1	**101100 | 111001010101**
Parent 2	**111100 | 010100110001**
Offspring 1	**101100 | 010100110001**
Offspring 2	**111100 | 111001010101**

Table 17: Example of one-point crossover for a binary encoding

This type of crossover is the one currently implemented in the genetic algorithm for the rotation experiment.

7.4.2 Two-point crossover

Two-point crossover is similar to the one-point with the difference that two cutting points are selected and then the interchanges between the parents are made starting from these crossovers. Table 18 illustrates the operation.

Parent 1	**101100 | 1110010 | 10101**
Parent 2	**111100 | 0101001 | 10001**
Offspring 1	**101100 | 0101001 | 10101**
Offspring 2	**111100 | 1110010 | 10001**

Table 18: Example of a two-point crossover for a binary encoding

7.4.1 Uniform crossover

In this type of crossover an operator is initially defined which decides the probability of the mixing ratio, that is the measure in which the parents will singularly contribute to the offspring. The mixing in this case is more at the allele level than at the segment level, as shown in

Parent 1	**1 0 1 1 0 0 1 1 1 0 0 1 0 1**
Parent 2	**1 1 1 1 0 0 0 1 0 1 0 0 1 1**
Offspring 1	**1 0 1 1 0 0 1 1 0 0 0 0 0 1**
Offspring 2	**1 1 1 1 0 0 0 1 1 1 0 1 1 1**

Table 19: Example of uniform crossover

Uniform crossover was deemed unadapt to the problem in exam since it was causing a fragmentation too high in the chromosomes, causing a complete change in the genes of a population from one generation to another one.

7.5 Mutation

Mutation is another genetic operator which takes place after the crossover operation. Its scope is to maintain genetic diversity from one generation to another. Mutation consists in altering one or more genes in a chromosome. Thanks to his operation, it is possible to replace genes lost during the evolution process and introduce new ones which were not present in the initial population. This could lead to have entirely new genes values in the gene pool (Chakraborty 2010).

As well as for the crossover operator, a mutation probability rate exists represented by the ratio of genes subjected to mutation at each iteration and the total number of genes. It determines the speed at which new genes are introduced into the population: a low rate would prevent the introduction of several genes that would increase the performance of the population; with an high rate, the quantity of random perturbations introduced decreases the similarity of the offsprings with the parents and the algorithm loses the experience gained in the previous iterations concerning the history of trials made in the research of the optimum. Hence, it is fundamental to find a good trade-off when choosing this parameter and often a low value is preferable, such as 0.01.

7.6 Advantages and disadvantages of GAs

Genetic algorithms presents several advantages, one for all the capability of examining a large search space. Whenever bad solutions are encountered during the evolution of the population, these are discarded and do not invalidate the result. The great property of GAs is that they are inductive processes, that is no knowledge on the rules of the problem are required. This characteristic is fundamental when dealing with complex or poorly defined problems (Jacobsen s.d.).

Unfortunately, the fact that genetic algorithms work through the theory of evolution processes could also lead to some drawbacks too. In fact, it is not given for granted that the evolution drives to the optimal solution but only avoids the bad ones. This behaviour could lead to local optima than the global one.

7.7 Preliminary simulations results

Several simulations were run trying different settings in terms of crossover rates and elitism. Finally, a good compromise was reached imposing an elitism equal to 10% of the population and a crossover rate of 80%. At the moment no mutation probability has been set since the approach employed for the selection foresees that a certain number of random individuals are added at each iteration.

The initial population is composed by 60 chromosomes where each chromosomes is composed by 30 image pairs. The results of the simulation are depicted in Figure 29 and Figure 30. In the first one the displacement of the image pairs in the final population are shown in order to observe whether a particular trend is visible. Moreover, in order to show the best solution of the initial population and the final one are shown, respectively highlighted in red and green. Unfortunately, when looking at the sparse disposition of the final generation it is not possible to drive particular conclusions on the areas that are more favourable for the observations. This is completely understable since the release of the software is only a preliminary and some

assumptions have been made in the process, one for all the estimation software used for the computation of the fitness needs the be substituted with the official one.

Despite that, when looking at Figure 30 it is possible to appreciate the positive evolution of the average and maximum fitness of the population at each iteration. Starting from an initial value rather low, as the iteration of the genetic algorithm proceeds an increase in the fitness is clearly visible until the curve approaches the asymptote of 1 representing the maximum fitness. This gives a good feeling regarding the capability and efficacy of genetic algorithms of optimizing the problem although the software still needs a lot of improvements and refinements.

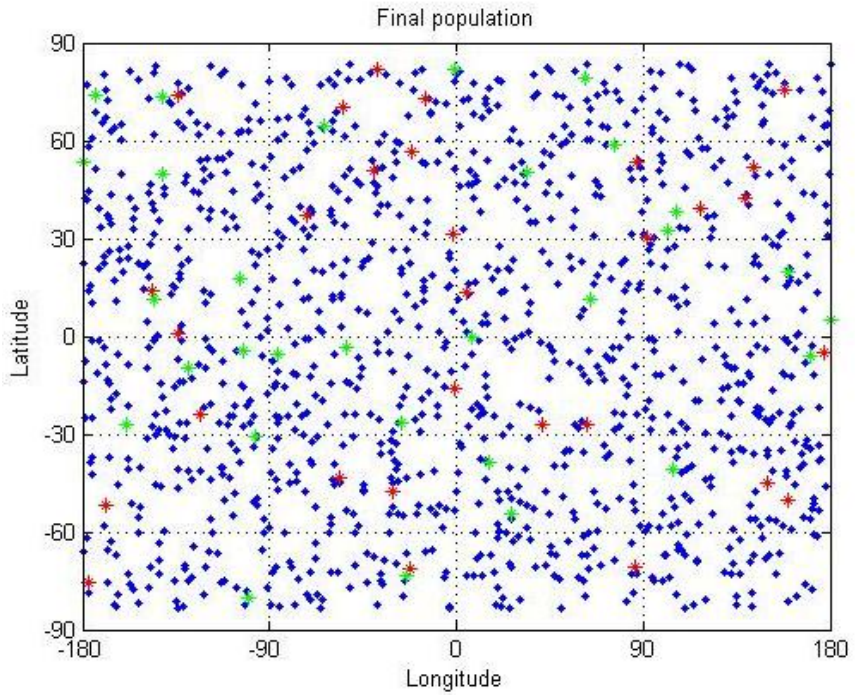

Figure 29: Preliminary simulation results of the genetic algorithm

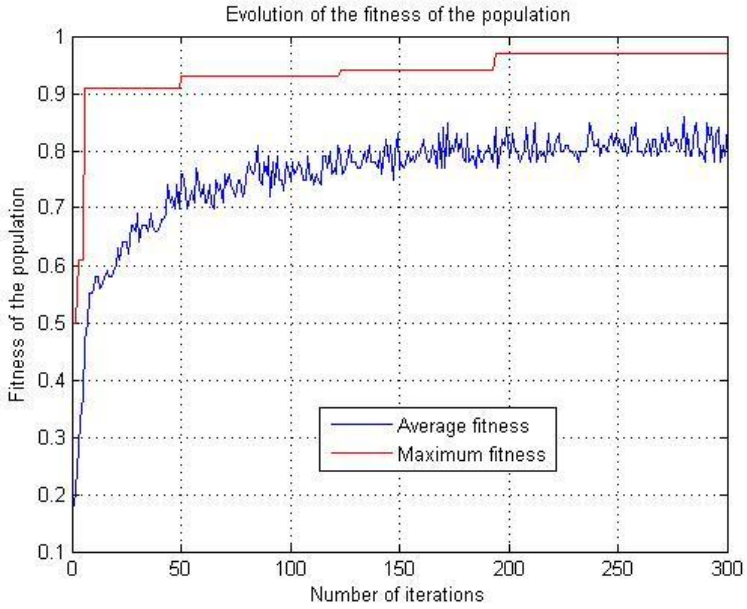

Figure 30: Evolution of the average and maximum fitness of the population

Chapter 8

Estimation procedure

In this chapter the simple model developed for the estimation of the rotational parameters is illustrated. As already stated in section 4.3, the implementation of this module is under the responsibility of the University of Rome where the complete model taking into account all the relevant parameters is under development. Despite that, in this first phase it was necessary to deal with a very simple software, able to return an output in very short computational times so as to facilitate the debugging of the optimization software. For this reason, a simple estimator was built that could be employed for the computation of the fitness function inside the genetic algorithm developed for optimizing the problem.

8.1 Mercury's orientation model

Since the aim of the estimation software is the retrieval of Mercury's rotational parameters obliquity and libration amplitude, the first step is the definition of the planet orientation with respect to an inertial frame. In Figure 31, the graphical illustration showing the parameters defining the orientation of a planet are shown (Davies, et al. 1980).

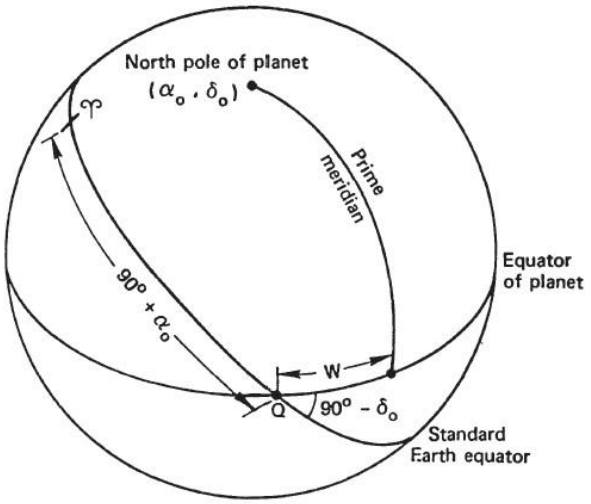

Figure 31: Reference system used to define the orientation of the planet (Davies, et al. 1980)

8.1.1 Reference system

In order to be able to identify the rotation of the planet two reference frames must be defined: an inertial and a body-fixed one. The body-fixed reference frame is invariant with respect to the surface characteristics and is defined to move with respect to one inertially fixed by the obliquity angle and rotation on its axis.

Hence, a rotation matrix between the frames is defined as follows:

$$R = R_2(-\varepsilon)R_3(-\theta) \tag{8.1}$$

Where ε indicates the obliquity angle and R_2 a rotation around the y axis, θ represents the current angle of Mercury's rotation at a certain epoch and R_3 indicates that this rotation is performed around the z axis. The information relative to the libration amplitude is contained in the angle θ as it will be more extensively explained in the following paragraphs.

8.1.2 Mercury's rotation

The rotational period of Mercury, that is the time it employs to accomplish an entire rotation of 360° around its axis, is about 58 days. Apart from this uniform motion, Mercury's rotation is also influenced by torques acting on its body and causing oscillations called librations, as seen in section 3.3.

In this treatise the forced annual librations induced by the Sun gravity torque insisting on Mercury's equatorial bulge are taken into consideration. The following expression is adopted for describing the libration angle:

$$\Lambda(\mathrm{t}) = \lambda_0 \sin MA \tag{8.2}$$

Where λ_0 is the libration amplitude and MA the Mercury mean anomaly.

Hence, the Mercury rotation is described by the angle $\Theta(t)$, sum of the contributions given by the nominal rotation and the librations as shown by the following relationship:

$$\begin{aligned} \Theta(t) &= \theta_0 + \omega t + \Lambda(\mathrm{t}) \\ &= \theta_0 + \omega t + \lambda_0 \sin MA \end{aligned} \tag{8.3}$$

Where θ_0 is the angle allowing that at perihelion the condition where Mercury's minimum axis of inertia is aligned with the Mercury-Sun direction is verified.

8.1.3 Rotational parameters estimation and Least Squares Method

A software was implemented for the estimation of the rotational parameters. This routine is employed inside the optimization procedure to infer the fitness of a population for the current iteration of the genetic algorithm.

The inputs received by the routine are listed in Table 20. A matrix containing all the data relative to the image pairs to be used is loaded, from the first couple to the number n, a parameter that can be set as desired in the simulation settings.

Estimation software inputs					
Observation (#)	**Observed feature coordinates on the surface**	**Epoch at the first observation**	**Epoch at the second observation**	**Mercury true anomaly at first observation**	**Mercury true anomaly at second observation**
1	$(x, y, z)_{BF}$	$ET_1\|_1$	$ET_2\|_1$	$MA_1\|_1$	$MA_2\|_1$
…	…	…	…	…	…
n	$(x, y, z)_{BF}$	$ET_1\|_n$	$ET_2\|_n$	$MA_1\|_n$	$MA_2\|_n$

Table 20: Inputs of the estimation software

For each couple the coordinates of the feature (or better said the subprobe point) on the surface are retrieved from the database, so its position in a Mercury fixed reference frame is known. This information is fundamental in order to compute the observables. Furthermore, the epochs at the which the first and second observation of the couple are taken and the Mercury's mean anomaly as well are passed to the program.

Once the coordinates of the landmarks on the surface are known the computed and observed observables can be derived. Computed observables are the ones obtained from the predicted model using estimated values of the librations and obliquity, the values that are supposed to be adjusted at the end of the simulation. Observed observables as well are simulated since real values are not available and the simulation is made considering the libration amplitude and the obliquity from the observations by Margot (Margot, et al. 2007), currently the most accurate ones.

The observed observables are computed through the following relationships:

$$x_{ine\,t1} = R_2(-\varepsilon)R_3(-\theta_1)x_{bf} \tag{8.4}$$

$$x_{ine\,t2} = R_2(-\varepsilon)R_3(-\theta_2)x_{bf} \tag{8.5}$$

where the rotation matrices taking into account the rotation angle computed for the two different epochs are used. Actually, the implementation takes advantage of the property of orthogonal matrices for which the following expression is valid:

$$R^T(\alpha) = R(-\alpha) \tag{8.6}$$

Hence, the previous formulas can be rewritten as:

$$x_{ine} = R^T{}_3(\alpha)R^T{}_2(\varepsilon)R^T{}_3(\theta)x_{bf} \tag{8.7}$$

The angles θ_1 and θ_2 are computed as follows:

$$\theta_1 = \theta_0 + \omega t_1 + \lambda_0 \sin MA_1 \tag{8.8}$$

$$\theta_2 = \theta_0 + \omega t_2 + \lambda_0 \sin MA_2 \tag{8.9}$$

Finally, the observable $\Delta\bar{x}$ can be computed as the difference from the inertial vector of the feature at the first epoch and the one at the second epoch:

$$\Delta\bar{x} = x_{ine\,t1} - x_{ine\,t2} \tag{8.10}$$

Since the observed observables should represent the real ones that will be taken in the future during the mission the noises coming from the error models are added. These errors consist in attitude error, position error, time tagging and pattern matching uncertainties.

The attitude error represent the misalignment of the camera with respect to the nominal nadir pointing due to uncertainties in the reconstructed spacecraft orientation. Accuracies under the threshold of 2.5 arcsec are expected. Unlike the position error, in this the maximum error is at apoherm, about 18.3 m on the surface, and minimum at periherm, 4.8 m.

A discrete error due to the wrong image time-tagging on board the S/C of the order of 10^{-3}s are considered. The associated error vector is given by the product between the ground velocity vector of the S/C per step time. A displacement of 2.58 m at periherm and 1.34 m at apoherm is obtained.

Another error source to be accounted for originates from the systematics, even if this contribution is currently not taken into account. In fact, the different illumination conditions acting on the probe cause thermoelastic deformation of the structure, especially on the optical bench where the camera is lodged. The effect is a misalignment of the camera for which the error is estimated to be less than 2 arcsec.

Although pattern matching errors depend on the algorithms employed, maximum sub pixels errors of the order of 10^{-1} are envisaged, as shown in Chapter 9.

The procedure for calculating the computed observable is totally analogous but instead of using the presumed correct values of libration and obliquity, initial guess values $\hat{\varepsilon}$ and $\hat{\lambda}$ are chosen:

$$\hat{x}_{ine\,t1} = R_2(-\hat{\varepsilon})R_3(-\hat{\theta}_1)x_{bf} \tag{8.11}$$

$$\hat{x}_{ine\,t1} = R_2(-\hat{\varepsilon})R_3(-\hat{\theta}_1)x_{bf} \tag{8.12}$$

The computed observables are then calculated:

$$\Delta\hat{x} = \hat{x}_{ine\,t1} - \hat{x}_{ine\,t2} \tag{8.13}$$

The problem will be solved by means of a least square method so the residuals must be computed:

$$r = \Delta\bar{x} - \Delta\hat{x} \tag{8.14}$$

Successively, the least square problem is defined. The objective of this algorithm is to solve the following system:

$$Ap = r \tag{8.15}$$

where A is the $m \times n$ Jacobian matrix of the partial derivatives, with m is the number of observations and n is the number of parameters to be estimated, p is a column vector of the parameters to be estimated and r is the vector of the residuals.

The matrix A is obtained as follows:

$$A_{ij} = \frac{\partial \Delta\hat{x}_i}{\partial p_j} \tag{8.16}$$

Where $i = 1,..,3$, (one for each component of the vector) and then repeated n times, that is the number of the observations. The matrix A then results to be equal to:

$$A = \begin{bmatrix} \frac{\partial \Delta\widehat{x_1}}{\partial \varepsilon} & \frac{\partial \Delta\widehat{x_1}}{\partial \lambda} \\ \cdots & \cdots \\ \frac{\partial \Delta\widehat{x_n}}{\partial \varepsilon} & \frac{\partial \Delta\widehat{x_n}}{\partial \lambda} \end{bmatrix} \tag{8.17}$$

While the final system is expressed by the following:

$$\begin{bmatrix} \frac{\partial \Delta\widehat{x_1}}{\partial \varepsilon} & \frac{\partial \Delta\widehat{x_1}}{\partial \lambda} \\ \cdots & \cdots \\ \frac{\partial \Delta\widehat{x_n}}{\partial \varepsilon} & \frac{\partial \Delta\widehat{x_n}}{\partial \lambda} \end{bmatrix} \begin{bmatrix} \varepsilon \\ \lambda \end{bmatrix} = \begin{bmatrix} \Delta\overline{x_1} - \Delta\hat{x}_1 \\ \cdots \\ \Delta\bar{x}_n - \Delta\hat{x}_n \end{bmatrix} \tag{8.18}$$

Where:

$$\Delta\hat{x} = R_2(-\hat{\varepsilon})\left[R_3\left(-\hat{\theta}_{t_1}\right)x_{BF} - R_3\left(-\hat{\theta}_{t_2}\right)x_{BF}\right] \tag{8.19}$$

The partial derivatives of the observable with respect to the parameters to be estimaed:

$$\frac{\partial\Delta\bar{x}}{\partial\varepsilon} = (-1)\frac{\partial R_2(-\varepsilon)}{\partial\varepsilon}\left[R_3\left(-\theta_{t_1}\right)x_{BF} - R_3\left(-\theta_{t_2}\right)x_{BF}\right]$$

$$\frac{\partial\Delta\bar{x}}{\partial\lambda} = R_2(-\varepsilon)\left[\frac{\partial}{\partial\lambda}[-\theta_{t_1}]\frac{\partial}{\partial\theta}R_3\left(-\theta_{t_1}\right)x_{BF} - \frac{\partial}{\partial\lambda}[-\theta_{t_2}]\frac{\partial}{\partial\theta}R_3\left(-\theta_{t_2}\right)x_{BF}\right] \tag{8.20}$$

After the solution of the rotational parameters is completed the fitness function for the current population is evaluated on the base of the accuracy obtained for the libration and the obliquity.

Chapter 9
Elaboration of the images

As already explained diffusely in the presentation of the research activity the good completion of this work and the experiment itself are strictly connected to the process of elaboration of the images collected by the onboard camera HRIC. Furthermore, the contribution in this field also extends to the mission planning phase as evident from the end-to-end simulator flowchart depicted in Figure 9 and illustrated in section 4.3.

For this reason the MORE team considered to establish a profitable collaboration with the Computer Vision Group of the University of Bologna, held by prof. Bevilacqua, with years of experience concerning the development of pattern matching algorithms and processing of the images and already collaborating with the Unibo team in occasion of previous projects.

9.1 Elaboration of the images

In the frame of the rotation experiment the image elaboration substantially intervenes in two different phases.

During the pre-mission phase, the one preceding the arrival of the probe to Mercury, it is used to drive the scientific planning of the observations providing valuable outputs for the optimization procedure of the global simulator. Instead, as soon as the real images collected by HRIC will be available pattern matching algorithms implemented ad-hoc for the particular condition under exam will be employed.

At the first stage the study on the elaboration of the images works in parallel with the observations software providing a database of crossovers on the surface. The aim is not only the problem of correlating the pairs employing the more adapt pattern matching algorithm, which is by the way one of the unknowns under investigation, but the determination of the pattern matching

error associated to the correlation process. In order to do so, the necessity arose of developing a software tool able to generate synthetic images simulating the real ones.

The Digital Elevation Model (DEM) would take as input the set of image pairs selected for the current iteration of the optimization procedure along with the information relative to lighting conditions and altitude of each observation and generate the synthetic image, while the rotational model would simulate the relative displacement and rotation between the images forming one pair.

The important breakthrough given by introducing such an instrument in the global simulator is the opportunity of using in the pattern matching procedure the real images, in terms of illumination conditions and scales. Hence, the true difficulty due to adverse conditions at which the image was taken and the problematic comparison of images differing too much can be tested exploring a set of diverse techniques and algorithms. Moreover, this could provide an authentic idea of the potentialities of the actual algorithms or if some limitations must be imposed to the couples of images that can be processed.

Due to the strict collaboration with the CVG team during the development of the global simulator and since an explanation of the image elaboration process could provide a better understanding of the present research and the rotation experiment in general, in this section a summary of their activity is reported. First, the implementation of the DEM is explained, followed by examples of its application in concrete cases employing a certain type of pattern matching algorithms.

9.2 Implementation of the synthetic image generator

In order to generate synthetic images as much as possible similar to the real ones, a digital elevation module simulating the surface roughness of Mercury and its superficial characteristics in terms of craters, plains, etc…, was implemented.

The overall process can be described by the following stages:

i. *The main coarser irregular surface is generated*
   This represents the base level texture of the surface and is generated by means of a fractional Brownian motion (fBm) algorithm employing a pink noise $\frac{1}{f^n}$
ii. *A random number of craters is added*
   The size of the craters can be set as input parameter and their shape is defined according to a Gaussian model. An analogous model is used to build the irregularities of the border on the top
iii. *Previous steps are repeated for each scale until the desired number of iterations is reached*

At each iteration the argument n of the pink noise in the first step is increased

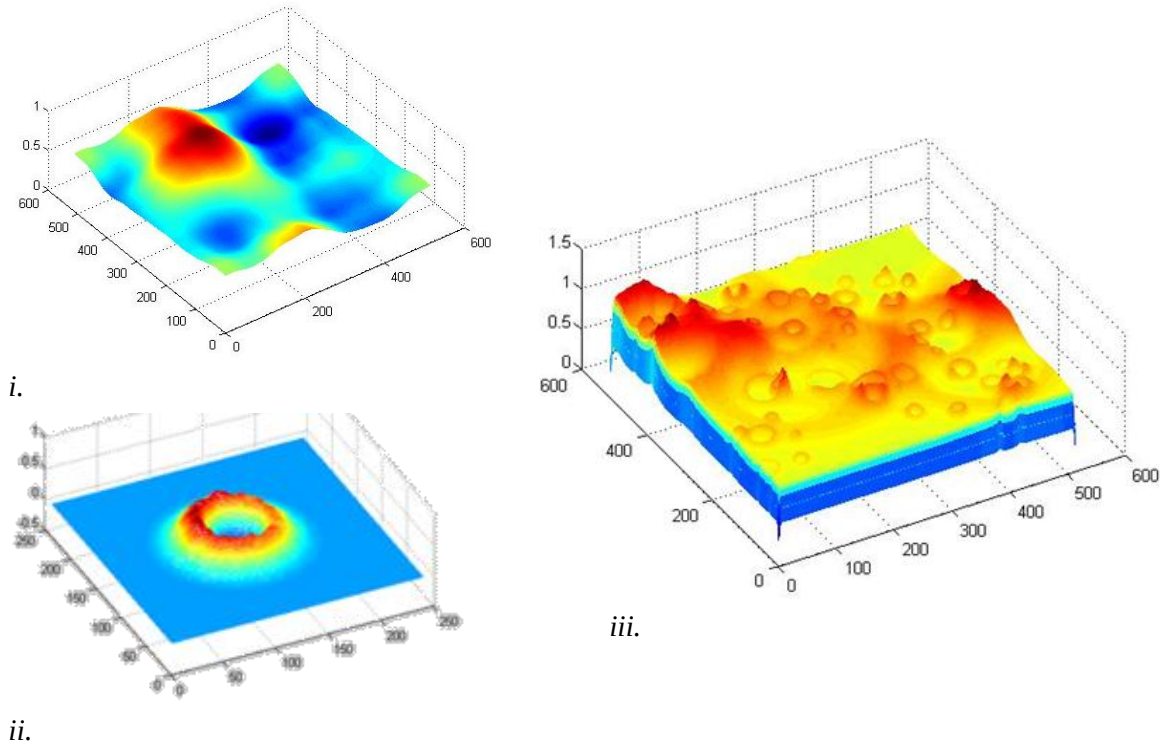

Figure 32: Synthetic image generation process

Illustration of the procedure for the generation of a Digital Elevation Module reproducing the surface of Mercury. i. the coarser texture of the surface is defined employing a pink noise; ii. a random number of craters with variable diameter size and modeled according to a Gaussian shape is added; iii. Step i. and ii. are repeated until the desired modeling of the surface is obtained

In order to add craters with plausible dimensions the data acquired by the previous missions Mariner 10 and MESSENGER have been studied, so as to obtain an estimate of the real sizes. Unfortunately, there exist no images taken at a resolution comparable with the one of BepiColombo. Anyway, it is very likely that the surface is populated with small craters and terrain features also at scales smaller than the resolutions available at the time being.

9.3 Ray tracing

The generated DEM is successively subjected to a rendering in order to obtain the final synthetic image by means of a ray-tracing software. Until now, the parameters that have been taken into consideration are the illumination conditions and the altitude of the spacecraft.

The Sun direction is modeled according to elevation and azimuth angles, both provided by the observations software as ancillary information of the crossover first defined in terms of latitude and longitude. The altitude is instead simulated introducing a zoom acting in the field-of-view of

the camera. Moreover, the camera FOV is deemed to be narrow enough so that the curvature of Mercury in the pictures is not appreciable.

For the moment the camera has been implemented as a simple pinhole. This model will be substituted in the future to be adapted to a more realistic structure which considers the HRIC parameters. It is very important that distortions of the lenses are taken into account in order to avoid accuracy errors.

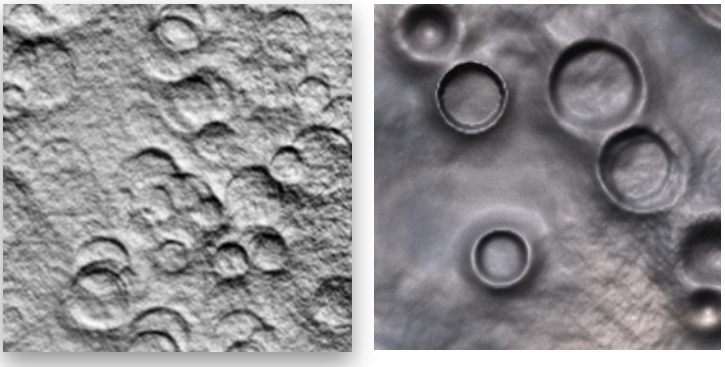

(a) Synthetic image **(b) Synthetic image**

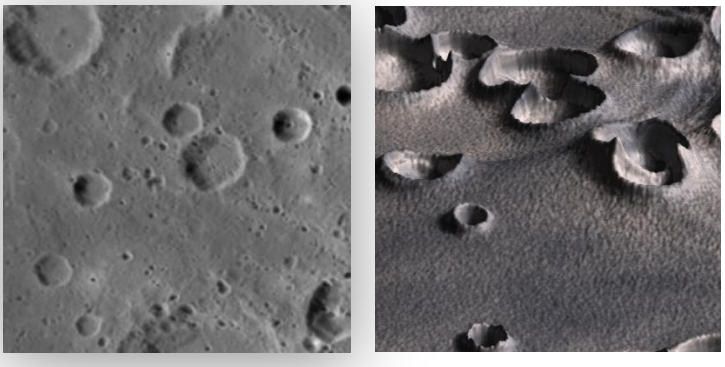

(c) MESSENGER **(d) Off-nadir synthetic image**

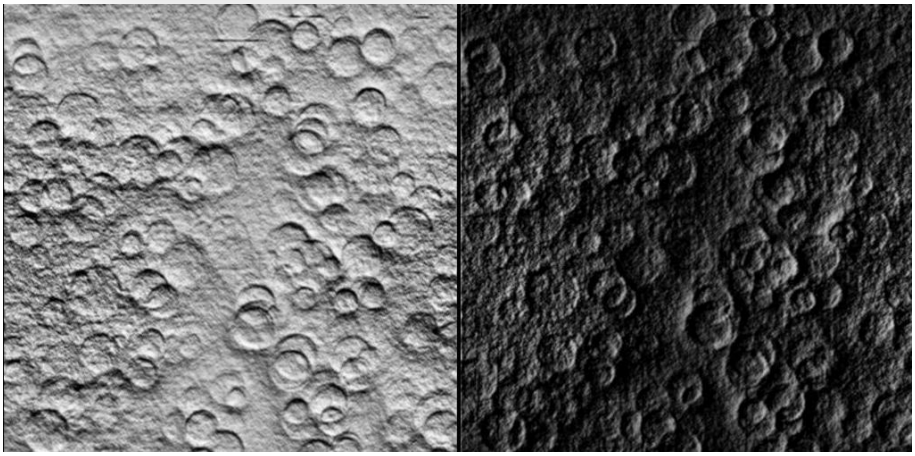

(e) Two rendered images of the same DEM using different phase angles

Figure 33: Examples of rendered images

In (a), (b) rendered DEMs employing different illumination angles are shown while (d) represents a rendering obtained imposing an off-nadir angle; (c) in order to compare the rendered images with a real one a picture

collected by the MESSENGER spacecraft is displayed; (e) to have an idea of the different appearance of two images

9.4 Pattern matching algorithms

The ultimate output of the analysis of image processing should be the definition of a limited set of pattern matching algorithms able to deal with the conditions that will be encountered in the real images. What is expected is that some scenarios in terms of differences in illuminations and scales between the images will repeat and each of them must be treated with a specific strategy in order to obtain the best accuracies.

Parameters / PM method	Δ Altitude	Δ Elevation	Δ Azimuth	Notes
Scale Invariant "Gradient Based" features (SIFT, SURF)	High	Limited	Very limited	No dependence on surface features
Geometric features	Moderate	Moderate	Limited*	Preprocessing required
Transformed Feature Space + Combined Matching and Shape from Shading	Moderate**	High	High	Preprocessing required

* Depending on the processing and its effects on the extracted shape/descriptors
** Post-processing required to build pyramid schemes for multi-scale image representation

Table 21: Summary of pattern matching algorithms categorized according to the different conditions to be handled

In Table 21 a summary is presented where the pattern matching algorithms deemed to be the best candidate to deal with the different cases are categorized according to their advantages and disadvantages.

- *Scale invariant "gradient based features (SIFT, SURF,…)*
  These methods are more tailored to small variations in lighting conditions between the images. In fact, they are able to deal with limited changes in sun elevation angles and even more restricted variations in azimuth. The achievable accuracy is very good, up to 10^{-2} pixels, and the good property they possess is that as sparse descriptors they are not influenced by the superficial characteristics of the terrain, such as craters, ridges and so on.

- *Geometric features*

To base an algorithm on the morphological characterization of the surface, such as plateaus, cliffs, craters, moderate changes in illumination are needed. Furthermore, in order to attenuate them it is necessary to perform a preprocessing, which is also needed for the identification of craters ridges or centers or highlight other superficial features

- *Transformed feature space (Size functions, …) and combined matching and Shape From Shading (M&SFS)*
  These methods are the best candidates for dealings with image pairs also affected by abrupt changes in illumination

Until now, simulations were performed employing a SIFT method while it is foreseen to implement in a second stage other registration approaches.

Scale-invariant feature transform is an algorithm able to detect and describe local features in images. By analyzing an image with this method it is possible to extract interesting points identified as "feature descriptors" at different scales. As suggested by the name, SIFT present a good robustness to changes of scales and rotations as well. Unfortunately, they are not equally performing when dealing with changes in illumination. This is due to the fact that features are extracted at different scales of the image and basing on the intensity of pixels gradients. For this reason, a preprocessing was introduced employing a congruency filter to damp this effect.

In Figure 34 a graphical illustration of the process of feature extraction from a rendered DEM image is displayed.

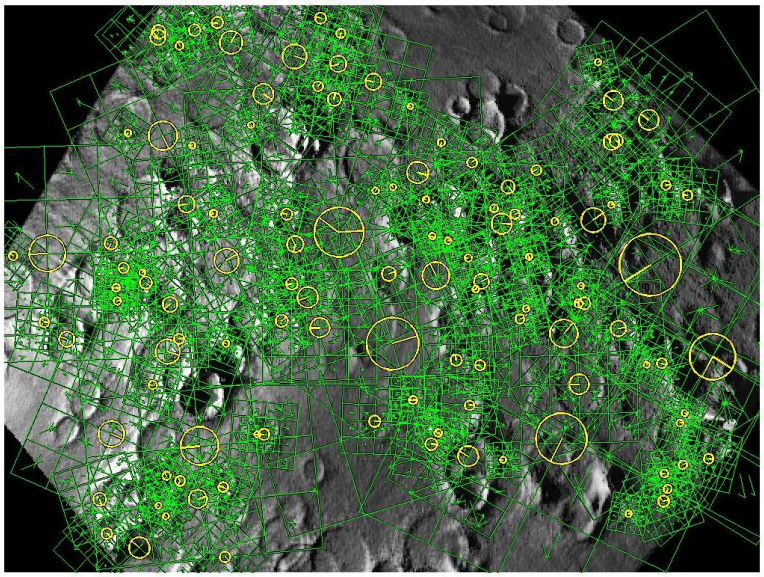

Figure 34: Graphical illustration of features extraction on rendered DEM by means of a SIFT algorithm

The same rendered image is then reused in the first example of Figure 35 where the application of pattern matching between image pairs are displayed.

In example (a) two images characterized more or less by the same scale and with slightly different illuminations are shown. Anyway, the difficulty presented in this case is the light coming with a very oblique to the surface thus causing an image considerably shadowed and obscure. Despite that, the algorithm is still able to identify and track the features in the images, capability that would not be reached with a cross correlation method, unable to deal this type of cases.

Case (b) is instead shown to demonstrate the goodness of the SIFT method for elevate variations in altitude as visible from the image. In fact, it is clear from the figure how the features can be tracked and identified in both images.

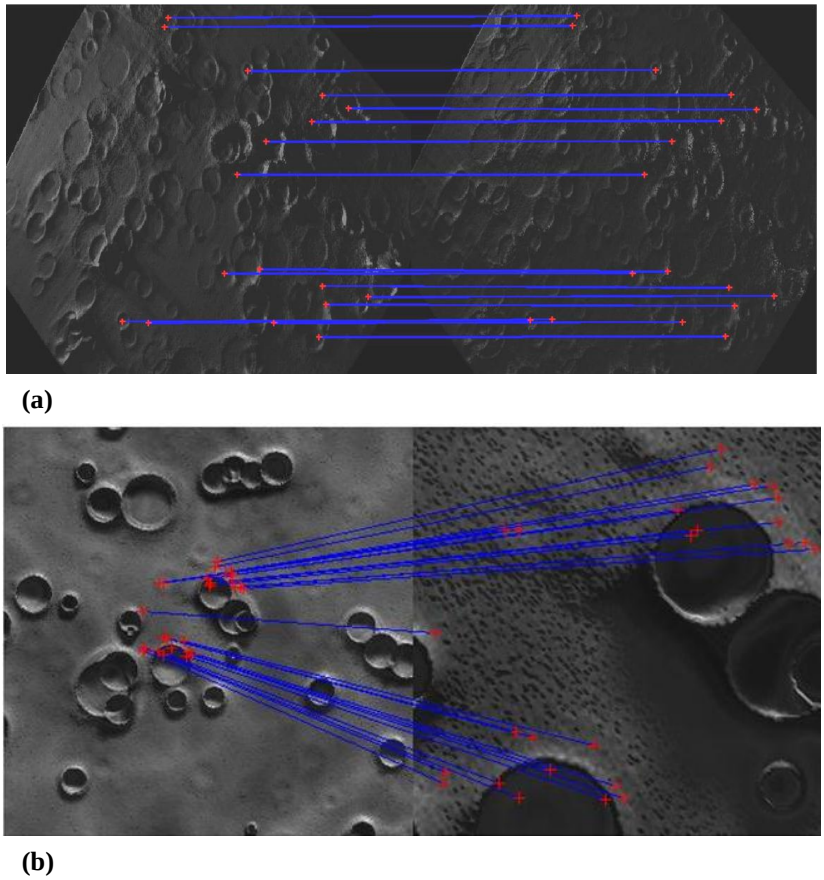

(a)

(b)

Figure 35: Examples of application of pattern matching employing a SIFT method

The accuracy of the tracking depends on the quality of the images, meant in terms of resolution, texture, noise, illumination, scale, etc. Considering the current state of the art of the pattern matching algorithms, accuracies of a minimum order of 10^{-1} pixels up to 10^{-2} pixels are obtainable. Examples of the outputs on the tracking accuracies are shown in Figure 36 and Figure 37. The implementation of such advanced techniques is not only beneficial for the capability of correlating 'problematic' images but indeed it also prevents the pattern matching error from being the one determinant for the noise affecting the observables.

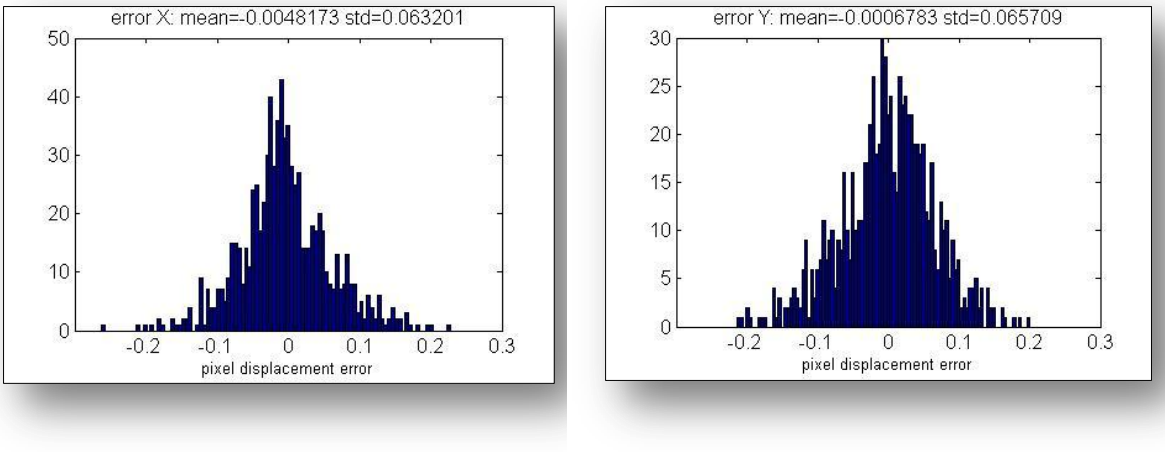

(a) **(b)**

Figure 36: Example of tracking accuracy results of 10^{-1} pixels

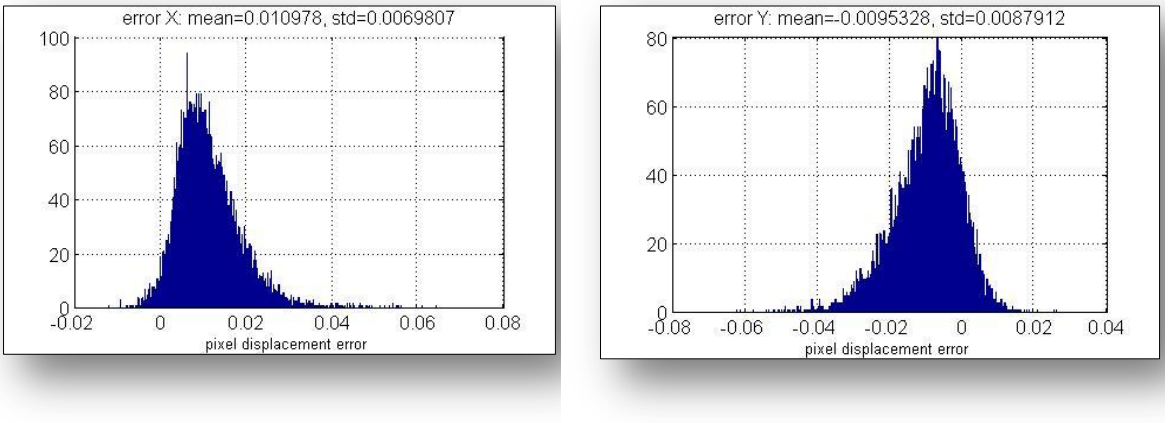

(a) **(b)**

Figure 37: Example of tracking accuracy results of 10^{-2} pixels

9.5 Super resolution

The super resolution is an observational strategy that allows to increment the potential resolution obtainable with a camera up to four times the original one.

As anticipated in section 6.1.1, this approach could be particularly advantageous in case a better quality of the images obtained at higher altitudes is needed so as to make them employable for the rotation experiment. This method could even be applied for building high-res mosaic maps, or on demand for analyzing interesting features or for visualization purposes.

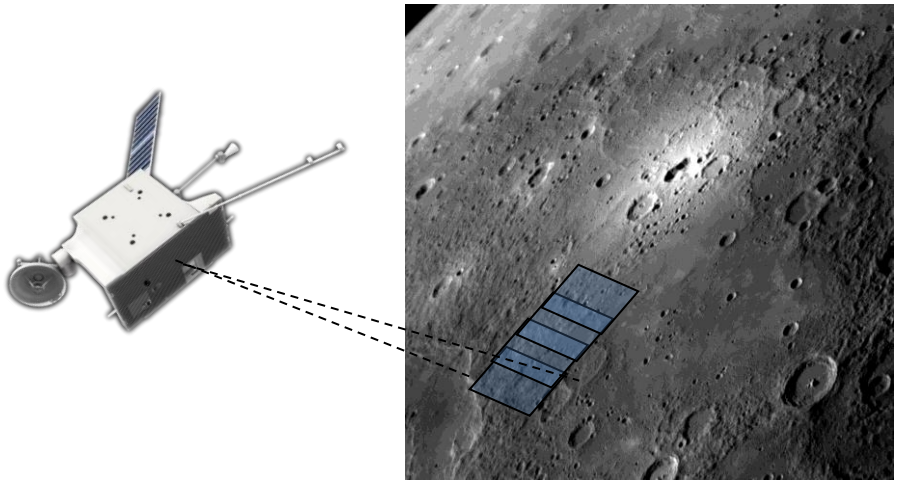

Figure 38: Super resolution technique

The technique is based on an oversampling of the same region as illustrated in Figure 38. Hence, images of the same portion of the surface are taken and post-processed to enhance the resolution. This technique falls in the variant of multiple-frame super resolution methods. Sub-pixels shifts between multiple 'low' resolution images of the same scene. It creates an improved resolution image fusing information from all low resolution images, and the generated higher resolution image are better descriptions of the scene. Other single frame methods attempt to magnify the image without introducing blur and 'guess' what the probable appearance of the high resolution image should be.

A concrete example of the application of the super resolution is shown in Figure 39. At the extreme right of the figure is the original image used for the example. The quality of this one was artificially degraded until the blurred image depicted on the left was obtained. Then, the super-resolution algorithm was applied taking multiple images of this quality and the result is the image in center. As it is possible to notice, its resolution is significantly enhanced and the difference with the original one is almost unappreciable at a glance.

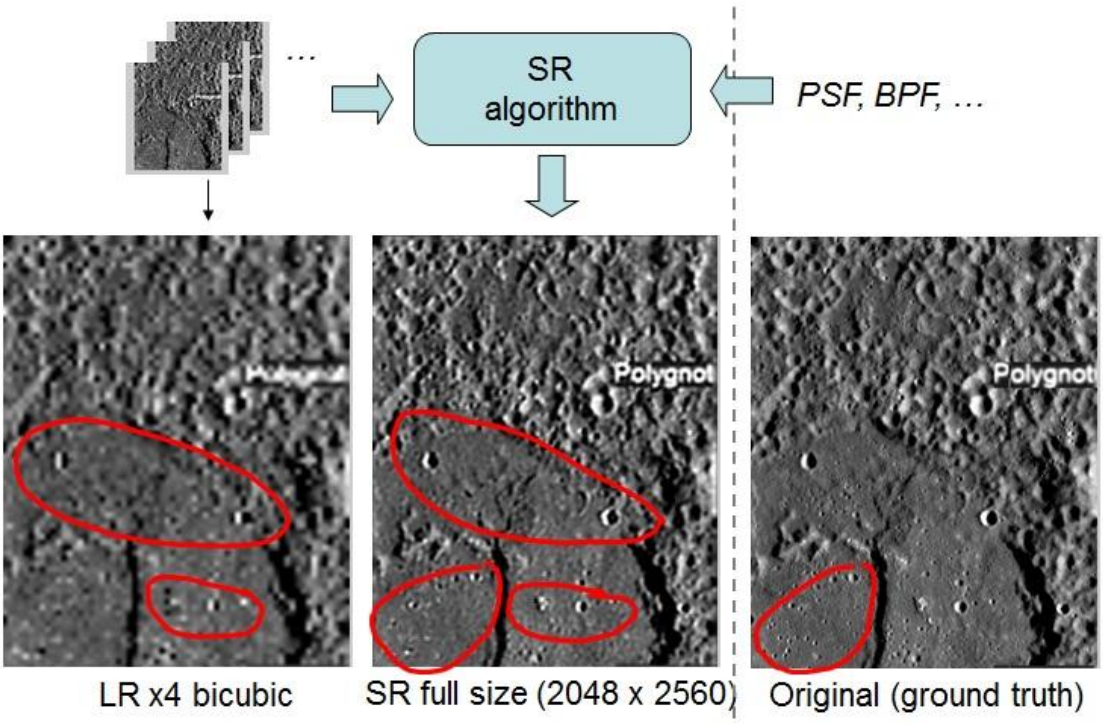

Figure 39: Example of application of the super resolution algorithm to enhance the quality of an image

References

n.d.

Anderson, J. D., G. Colombo, P. B. Esposito, E. L. Lau, and G. B. Trager. "The Mass, Gravity Field, and Ephemeris of Mercury." *Icarus 71*, 1987: 337-349.

B. Bertotti, L. Iess, P. Tortora. "A test of general relativity using radio links with the Cassini spacecraft." *Nature* 425, no. 374-376 (2003).

Benkhoff, J. "BepiColombo: ESA's Mission to Explore Mercury." *EPSC - European Planetary Science Congress.* Nantes, 2011.

Chakraborty. *Genetic Algorithms - http://www.myreaders.info/09_Genetic_Algorithms.pdf.* 2010.

Colombo, G. "Rotational period of the planet Mercury." *Nature* 208 (1965): 575.

Colombo, G., and I. I. Shapiro. "The rotation of planet Mercury." *The Astrophysical Journal* 145 (1966): 296-307.

Davies, M. E., et al. "Report on the IAU working group on cartographic coordinates and rotational elements of the planets and satellites." *Celestial Mechanics*, 1980: 205-230.

DLR. n.d.

ESA Web Site - Cebreros Station. http://www.esa.int/esaMI/Operations/SEMVSDSMTWE_0.html.

Flamini, E., and et al. "SIMBIO-SYS: The spectrometer and imagers integrated observatory system for the BepiColombo planetary orbiter." *Planetary and Space Science* 58 (2010): 125-143.

Garcia, D., R. Jehn, J. Schoenmaekers, and P. de Pascale. *BepiColombo Mercury Cornerstone Consolidated Report on Mission Analysis.* BC-ESC-RP-05500, Issue 3.2, ESA/ESOC: Mission Analysis Section, April 2010.

Hoofs, R., H. Middleton, and J. McAuliffe. "BepiColombo Science Mission Operations Analysis." *BepiColombo Science Operations Working Group.* ESA/ESTEC, Noordwijk, 2010.

Iess, L., M. Mercolino, P. Persi, and P. Tortora. "BepiColombo Rotation Experiment." 2003.

Iess, L., S. Asmar, and P. Tortora. "MORE: An advanced tracking experiment for the exploration of Mercury with the mission BepiColombo." *Acta Astronautica* 65 (2009): 666-675.

Jacobsen, T. *Genetic algorithms, http://subsimple.com/aboutme.asp.* n.d.

Jorda, L., and N. Thomas. "The accuracy of pattern matching techniques for the radio science experiment of ESA's Mercury cornerstone mission." Preliminary study (not published), Max-Planck Institute for Aeronomie, Katlenburg-Lindau, Germany, 2000.

Margot, J. L., S. J. Peale, R. F. Jurgens, M. A. Slade, and I. V. Holin. "Large longitude libration of Mercury reveals a molten core." *Science* 316 (2007): 710-714.

Milani, A., A. Rossi, D. Vokrouhlicky, D. Villani, and C. Bonanno. "Gravity field and rotation state of Mercury from the BepiColombo Radio Science Experiments." *Planetary and Space Science* 49 (2001): 1579-1596.

Milillo, A., and et al. "The BepiColombo mission: An outstanding tool for investigating the Hermean environment." *Planetary Space Science* 58 (2010): 40-60.

Murray, B. C. "The Mariner 10 pictures of Mercury: an overview." *Journal of Geophysics* 80 (1975): 2342-44.

NASA Web Site - Cassini mission. n.d.

NASA Web site, MESSENGER mission. *http://messenger.jhuapl.edu/instruments/MDIS.html.* n.d.

Ness, N. F., K. W. Behannon, R. P. Lepping, Y. C. Whang, and K. H. Schatten. "Magnetic Field Observations near Mercury: Preliminary Results from Mariner 10." *Science 185*, 1974: 151.

Obitko, M. *Genetic algorithms - http://www.obitko.com/tutorials/genetic-algorithms/introduction.php.* 1998.

Peale, S. J. "Generalized Cassini's laws." *Astronomical Journal* 74 (1969): 483.

Peale, S. J. "Inferences from the dynamical history of Mercury's rotation." *Icarus* 28 (August 1976): 459-467.

Peale, S. J. "Rotational dynamics of Mercury and the state of its core." (F. Vilas, C. Chapman and M. Mattthews, University of Arizona Press, Tucson) 1988: 461-493.

Pettengill, G. H., and R. B. Dyce. "A radar determination of the rotation of planet Mercury." *Nature* 206 (1965): 1240.

Pfyffer, G. *Libration and obliquity of Mercury from the BepiCOlombo radio science and camera experiments.* Université catholique de Louvain: PhD Thesis, 2010.

Pfyffer, G., T. Van Hoolst, and V. Dehant. "Librations and obliquity of Mercury from the BepiColombo radio science and camera experiments." *Planetary and Space Sciences* 59 (2011): 848-861.

Team, MORE. "MORE Science Performance Report (SPR)." 2009.

Thomas, N., et al. "The BepiColombo Laser Altimeter (BELA): Concept and baseline design." *Planetary and Space Science* 55 (2007): 1398-1413.

Van Hoolst, T. "The Rotation of the Terrestrial Planets." *Teratise on Geophysics* 10 (2007): 123-164.

Van Hoolst, T., F. Sohl, I. Holin, O. Verhoeven, V. Dehant, and T. Spohn. "Mercury's Interior Structure, Rotation, and Tides." *Space Sci. Rev. 132*, no. 2-4 (2007): 203-227.